Intermittent streamflow generation in a merokarst headwater catchment

by

Camden M. Hatley

B.S., Arizona State University, 2020

A THESIS

submitted in partial fulfillment of the requirements for the degree

MASTER OF SCIENCE

Department of Geology
College of Arts and Sciences

KANSAS STATE UNIVERSITY
Manhattan, Kansas

2022

Approved by:

Major Professor
Dr. Matthew F. Kirk

Copyright

Abstract

Effective environmental protection strategies for intermittent headwater streams are dependent on first understanding the mechanisms that drive streamflow generation. Previous research in merokarst headwater catchments at the Konza Prairie Biological Station (KS, USA) indicate that intermittent streamflow is fed by multiple surface and subsurface water sources and that threshold behavior in the watersheds contributes to flow intermittency. However, we do not yet understand the relative contributions from each of the water sources nor the specific mechanisms governing the observed threshold behavior. In this study, we employed high-frequency chemical sampling of an intermittent headwater stream and groundwater in a merokarst watershed in the Konza Prairie Biological Station during the 2021 growing season. Our specific goals were to quantify the contributions to streamflow from different water sources, characterize their short-term dynamics, and uncover potential mechanisms behind flow intermittency.

Mixing calculations using stable water isotopes indicate that precipitation and surface runoff comprised < 5% of stream flow during most of the sampling period but could comprise > 50% at the peak of large storms when the stream was previously dry. Mixing calculations using major ions indicate that contributions from soil water were < 3% throughout the sampling period and that the dominant contributor was groundwater sourced from two separate perched limestone aquifers. Of the two, the shallower aquifer dominated streamflow generation over most of the study period (39% - 83%), but contributions from the deeper aquifer increased over periods of days to weeks when no precipitation occurred (16% - 60%). During the early period of the study, groundwater contributions from both aquifers were lower than expected based on

predictions from stream conditions and groundwater elevations. This discrepancy suggests that groundwater sources are not fully connected to the stream channel until a critical threshold of water storage in the aquifers is attained. Given the dominance of groundwater contributions to streamflow compared to other sources, we hypothesize that this subsurface storage threshold is a major controller of flow intermittency in merokarst headwater catchments.

Table of Contents

List of Figures

List of Tables

Chapter 1 - Introduction

Headwater catchments with intermittent streamflow are significant sources of water, nutrients, and energy for both human populations and natural ecosystems worldwide. According to previous studies, headwater streams are estimated to comprise 66% – 80% of total global stream length (Leopold, 1964; Naiman et al., 2005), and intermittent flow is estimated to account for 30% – 50% of total river discharge (Tooth, 2000; Datry et al., 2014). Despite their importance, however, there has been little research on the mechanisms behind streamflow intermittence, especially for small headwater catchments in grassland environments (Shook and Pomeroy, 2012; Costigan et al., 2015). The small size and high hillslope connectivity of headwater catchments (Benda et al., 2005) make them highly sensitive to environmental disturbances and thus particularly vulnerable to the effects of climate change and human developments (Jaeger et al., 2014), but effective management strategies for these intermittent landscapes cannot be developed and applied unless we understand the processes which route water through them (Datry et al., 2014). In this study we aim to characterize the sources and timings of streamflow generation in an intermittent headwater stream in order to further understanding of the mechanisms behind flow intermittency.

This study addresses a headwater catchment within the Konza Prairie Biological Station, hereafter referred to simply as Konza, in northeastern Kansas which is classified as a merokarst landscape. Merokarst landscapes are a subset of carbonate terrains in which thin, permeable carbonate units are interbedded with relatively impermeable mudstones. Despite the fact that a high proportion of carbonate terrains are merokarst, including significant parts of central North America (Macpherson, 1996; Weary and Doctor, 2014), they remain largely understudied compared to other carbonate terrains (Sullivan et al., 2020). The rapid transport of water

generally seen in carbonate terrains amplifies the sensitivity of the environment to disturbances (Ford and Williams, 2007), exacerbating the responsiveness of the headwater catchments in Konza.

Several studies have been conducted at Konza that reveal key pieces of information about streamflow generation and flow intermittency. Costigan et al. (2015) used long-term precipitation and discharge data (1987-2011) to characterize the overall hydrology of Konza and observed that headwater discharge patterns are disconnected from precipitation patterns. They concluded that threshold-driven processes were causing this disconnect and ultimately leading to intermittent flow behavior, and they offer the gradual closing of soil macropores and the filling of groundwater storage zones as two possible mechanisms that might be giving rise to the threshold dynamic.

Sullivan et al. (2019) conducted a mixing analysis on an intermittent stream in a headwater catchment at Konza and concluded that the stream water is a mixture of four different sources: surface runoff, soil water, groundwater flowing through the carbonate aquifers, and groundwater flowing along the carbonate-mudstone contacts. This analysis shows the utility of mixing analyses for identifying the potential water sources that contribute to streamflow generation, but it doesn't inform on the short-term dynamics of these sources that might help give rise to flow intermittency. Additionally, the mixing analysis uses a single averaged endmember composition for all groundwater sources, meaning that it does not capture separate contributions to streamflow from different perched aquifers within Konza bedrock. The different perched carbonate aquifers at Konza have significantly variable chemical compositions, meaning that shifting contributions from these aquifers to the stream can have a significant impact on stream chemistry (Macpherson, 1996; Wood and Macpherson, 2005). Furthermore, each

aquifer can have significantly different hydrogeologic properties (Pomes, 1995) and outcrop patterns, meaning that they might impart significantly different flow pathways on water moving through them.

In this study, we seek to build on these previous analyses by investigating the relative importance of different water sources, their variation on short time scales, and how this variation might influence stream flow intermittency. To achieve this goal, we used high frequency sampling of surface and groundwater at Konza during the 2021 growing season (April – July) to quantify streamflow source contributions and characterize their short-term dynamics. We collected stream samples on a weekly to hourly basis depending on flow conditions and applied various mixing analyses to capture small timescale changes to source contributions. We also utilized high frequency discharge, precipitation, and groundwater elevation data to provide context for any changes to source contributions and aid in interpretations of threshold-driven behavior that might be controlling flow intermittency.

Chapter 2 - Methods

2.1 Study Area

The study site for this project is watershed N4D within the Konza Prairie Biological Station (Konza) in northeastern Kansas (Figure 1). N4D is a 1.2 km^2 headwater catchment drained by an intermittent fourth order stream that flows into Kings Creek. The watershed is largely dominated by native prairie grasses that are regularly grazed by native bison. Woody vegetation including oak, hackberry, and elm grow within the riparian zone of the principal stream while other woody species like dogwood and sumac have significantly encroached up the catchment hillslopes since the inception of Konza (Veach et al., 2014). N4D is burned every four years as part of ongoing research on the connection between grassland burn frequency and woody encroachment, and the most recent burn occurred on April 12, 2021, three days before the first sample collection in this study.

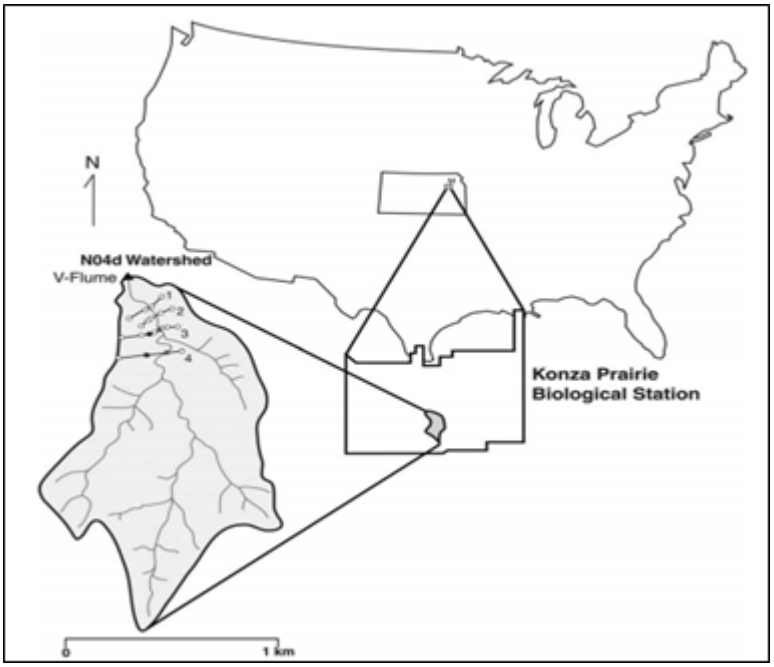

Figure 1. Location of Konza Prairie Biological Station and watershed N4D. Figure from Wood and Macpherson, 2005.

Konza receives an average of 835 mm of precipitation annually (Hayden, 1998). Of this precipitation, most of it falls during the growing season which roughly runs from April – September (Figure 2a) (Nippert, 2021). Discharge measured at a gauging station at the outlet of N4D peaks in May – June, coinciding with the peak of precipitation, but quickly dries out for the rest of the year despite the persistence of frequent precipitation over the remainder of the growing season (Figure 2b) (Dodds, 2021). This is likely due to vegetation reaching its maximum growth in mid-summer and achieving maximum rates of evapotranspiration, which is estimated to account for 75% of the total annual water budget in Konza (Steward et al., 2011).

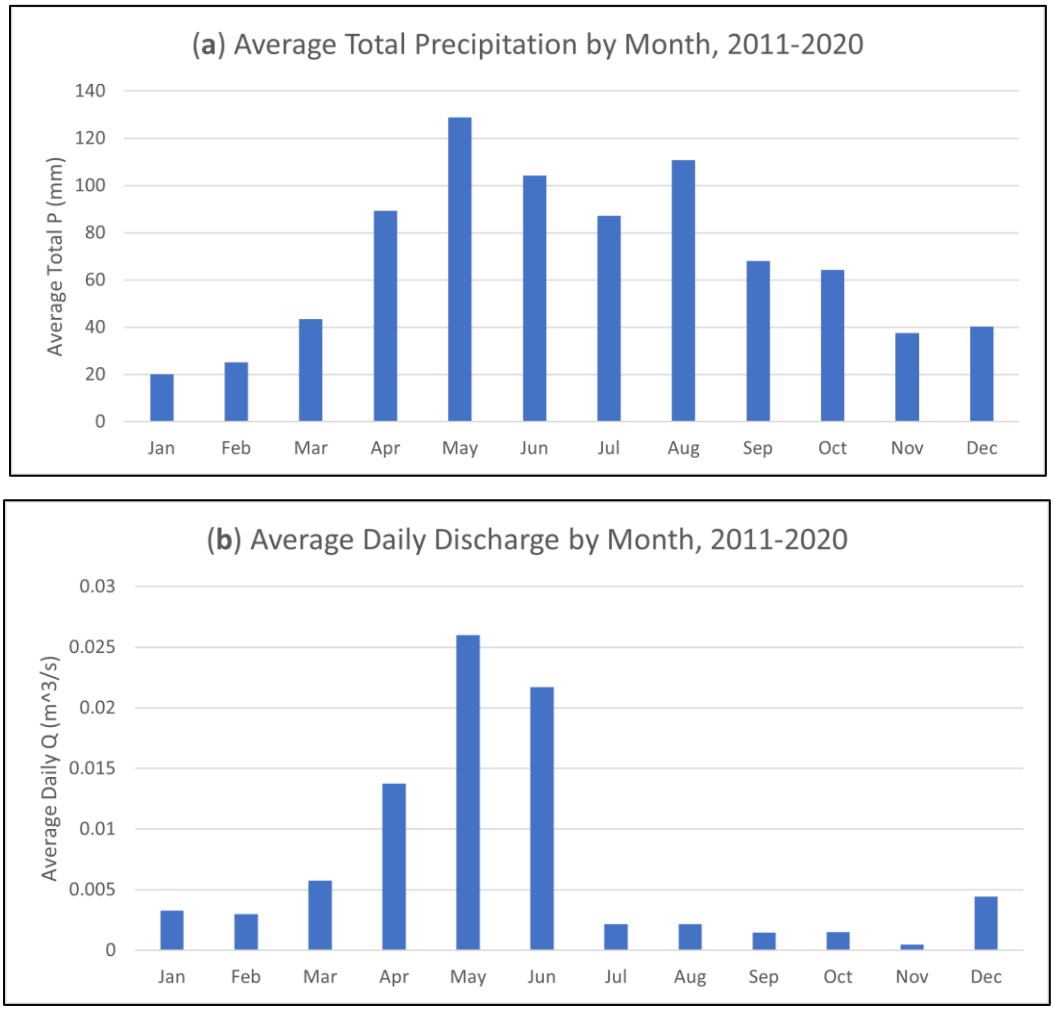

Figure 2. Average total precipitation (a) and average daily discharge (b) by month over the 10 year period 2011-2020. Data from Nippert, 2021 (a) and Dodds, 2021 (b).

The geology of N4D is characterized by an alternating sequence of nearly horizontal 1-2 meter-thick limestones and 3-4 meter-thick shales (Figure 3). There are 31 groundwater monitoring wells within the watershed which are drilled into the Eiss and Morrill limestones, which crop out in the lower 1/4th of the principal stream (Figure 4). The Eiss Limestone is divided into two hydrogeologically distinct units, referred to as the Upper and Lower Eiss. Five of the wells in N4D, including three in the Morrill and one each in the Upper and Lower Eiss, are equipped with pressure transducers which record groundwater elevation in the well every five minutes.

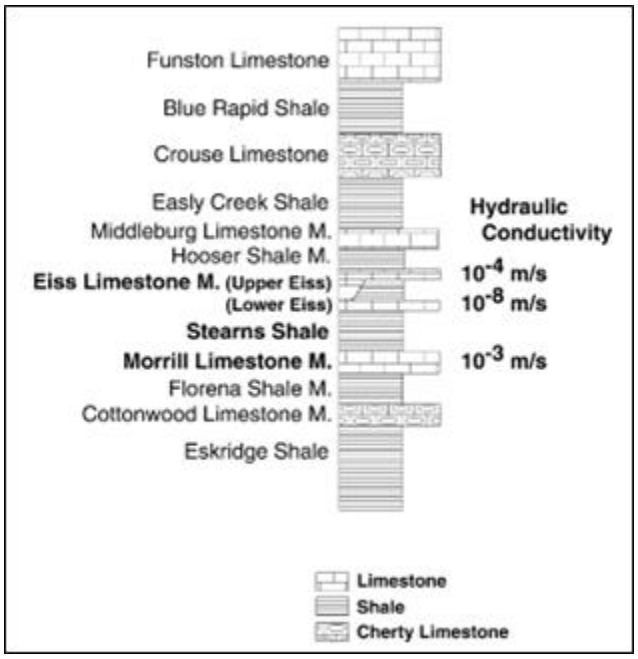

Figure 3. Partial stratigraphic column of Konza showing the units that crop out at watershed N4D. Bolded units are those that crop out in the lower 1/4th of the watershed, where this study is focused. Hydraulic conductivities measured in Pomes, 1995 are provided for the bolded units. Figure from Wood and Macpherson, 2005.

Previous slug tests returned hydraulic conductivities of 10^{-3} for the Morrill, 10^{-8} – 10^{-5} for the Lower Eiss, and 10^{-5} – 10^{-4} for the Upper Eiss (Pomes, 1995). While these hydraulic conductivity values provide an estimate for their respective units, groundwater flow within these limestone aquifers is mostly accommodated by fractures and solution-enlarged pores meaning

that true hydraulic conductivity within each unit likely has extreme spatial heterogeneity. Indeed, well productivity varies considerably from site to site within the same unit (Macpherson, 1996).

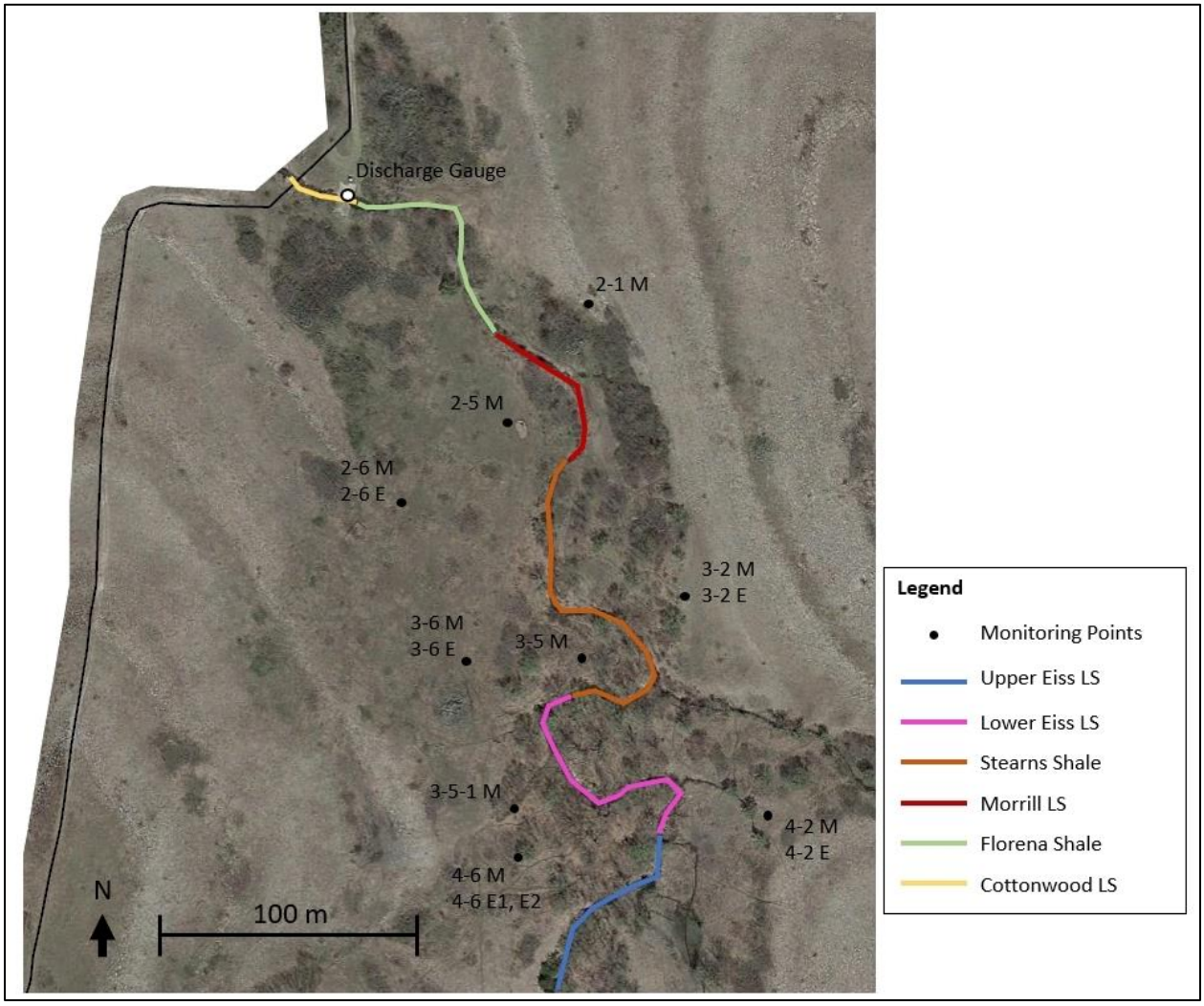

Figure 4. Overhead view of the lower 1/4th of N4D. Selected wells are marked with dots and labeled by the well number and the unit it is drilled in: M for Morrill, E for Eiss, and where the Eiss is differentiated, E1 for Lower Eiss and E2 for Upper Eiss. Pressure transducers are located in wells 3-5 M, 3-5-1 M, 4-6 M, 4-6 E1, and 4-6 E2. Stream reach is colored according to the outcropping unit. Location of the discharge gauge is labeled as the V-notch flume.

The current understanding of streamflow generation in the merokarst of Konza can be summarized into the following conceptual model. Streamflow is dominated by groundwater discharging from the bedded carbonate units in the merokarst sequence, but because the

impermeable mudstones restrict vertical movement of water between the carbonates, each carbonate bed acts as an isolated, perched aquifer with predominantly horizontal groundwater flow. Lithological differences between these aquifers can cause groundwater contained within each unit to have unique chemical compositions and flow properties (Macpherson, 1996; Wood and Macpherson, 2005). Recent studies have suggested that vertical flow between the carbonate units is much more significant than previously thought, but the full extent of this phenomenon is still not fully understood and is likely still limited compared to horizontal flow (Barry, 2018; Sullivan et al., 2020). Surface runoff into the stream can occur during storms, but it is likely limited in importance due to the presence of soil macropores and bedrock fractures which route precipitation into the subsurface instead (Figure 5) (Macpherson et al., 2008; Tsypin and Macpherson, 2012).

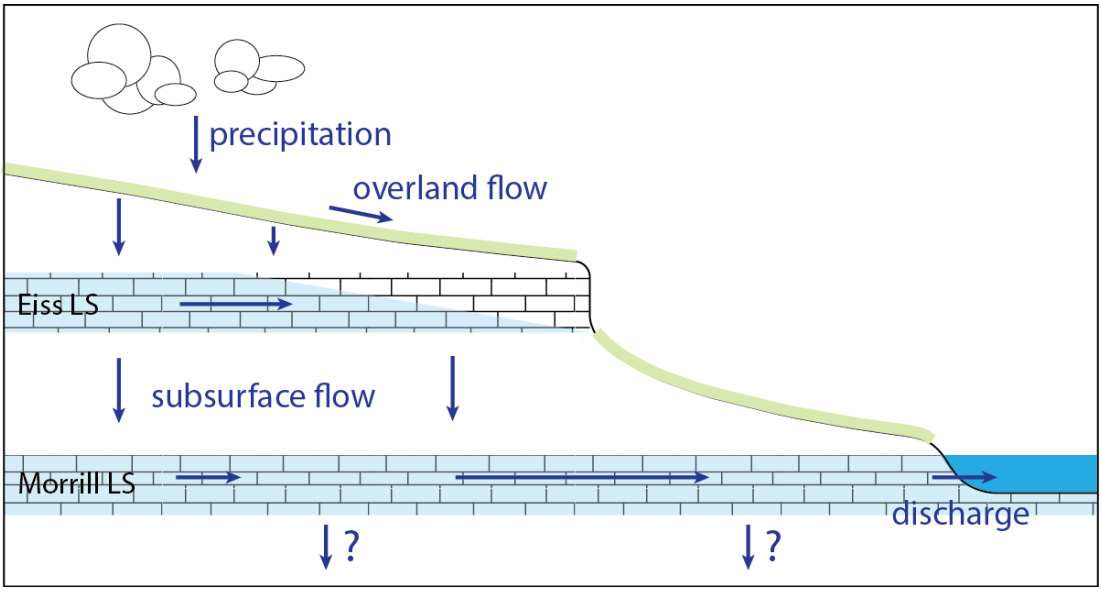

Figure 5. Conceptual model of streamflow generation in the merokarst terrain of a Konza Prairie Biological Station headwater catchment. Water falling as precipitation in the catchment can follow a variety of pathways, marked with blue arrows. The predominant pathway is horizontal flow within perched carbonate aquifers, designated with a brick pattern, but water can also reach the stream by running over the surface. Vertical movement between carbonate aquifers occurs and can export water out of the watershed entirely, but the extent of vertical flow is likely limited compared to horizontal flow.

Previous studies on the hydrogeology of N4D have shown that it is complex. The gauge at the outlet of the watershed frequently records no-flow all the way from July to February of the following year, but a portion of the principal stream experiences flow nearly perennially. This portion begins where the outcropping unit in the stream transitions from Upper to Lower Eiss and continues until the outcropping unit transitions from the Stearns shale to the Morrill. This suggests that under these flow conditions, the Eiss limestone is discharging water to the stream and the stream is then recharging water to the Morrill. Furthermore, groundwater elevations in the Morrill across the study area suggest the presence of a mound in the groundwater that disrupts the otherwise southward flow within the unit. The location, shape, and size of this mound can all change over time and are difficult to predict from flow conditions in the stream (Macpherson, 1996; Barry, 2018). While each limestone unit has generally been thought of as an isolated aquifer with limited flow between them, Sullivan et al. (2020) have shown that significant vertical transport of groundwater can occur in localized areas such as collapse features. Barry (2018) found direct evidence of this when a tracer dye injected in the Morrill limestone appeared in significant concentrations in groundwater discharging from the Cottonwood limestone, which is the next limestone underlying the Morrill and crops out immediately below the gauging station (Figure 4).

The complexity of the hydrogeology in addition to the extensive catalog of previous research make N4D an ideal location for the analysis in this study. While the potential flow pathways through the subsurface are hard to pin down, endmember mixing analysis provides a way of elucidating how water is moving through a catchment by first establishing endmember compositions and then sampling the water that discharges at the surface (Stewart et al., 2022). Establishing endmember compositions is accommodated in N4D via the wells that provide easy

access to the groundwater and the previously published data that provide long-term records of precipitation, surface, and groundwater chemistry. Through the high frequency sampling that we employed in this study, we aim to clarify aspects of N4D's hydrogeology by quantitatively describing streamflow generation.

2.2 Field Methods

In order to characterize the short-term dynamics of streamflow generation in N4D, we employed a high frequency sampling strategy for surface water, groundwater, and precipitation. The sampling period ran from 4/15/2021 to 7/16/2021 to coincide with the wet season when the stream had consistent flow. Surface water was collected from the stream immediately downstream of the flume at the catchment outlet. The frequency at which we collected stream samples varied based on the conditions in the watershed: during low flow conditions towards the end of the sampling period this frequency was roughly weekly, during the peak of the wet season this frequency was roughly daily, and during selected storms this frequency was roughly hourly. We selected five storms during the sampling period for hourly sampling which fell on 5/8-5/9, 5/26-5/27, 6/11, 6/24-6/25, and 7/15. These events were chosen to represent a range of storm intensities and antecedent watershed conditions, and we collected precipitation with a rain collector for each event. Sampling for these events began at the onset of precipitation and continued until approximately two hours after precipitation ceased. In total, 44 stream samples were collected over the 93-day sampling period.

For each stream sample, we first submerged field probes in the stream to measure water temperature, pH, conductivity, and dissolved oxygen. Probes were recalibrated for all parameters before each sampling trip. Immediately upstream of the probes, we filtered water through 0.45 µm syringe filters into collection bottles. We filled two 30 mL high density

polyethylene (HDPE) bottles for major ion concentrations, a 10 mL glass vial for stable water isotopes, and a 60 mL amber glass bottle for non-purgeable organic carbon and total dissolved nitrogen. One of the 30 mL HDPEs was used for anion analysis, and one for cation analysis; within a day of sample collection, we added three drops (100-150 µL) of trace-element grade HNO_3 to the cation bottle for preservation. We syringe-filtered precipitation samples in the same manner as stream samples, but only into the 10 mL glass vials for stable water isotopes. All samples were placed on ice for transport to the lab and then refrigerated until geochemical analysis.

We collected groundwater samples on six different days during the sampling period. For each groundwater sampling event, we collected water from the three wells in the 4-6 well nest (see Figure 5 for well locations). Each of these wells is completed in one of the three limestone aquifers which crop out in the lower reach of the stream: the Morrill, Lower Eiss, and Upper Eiss limestones. On three of the sampling events, groundwater was also collected from the 3-5 and 3-5-1 wells which draw from the Morrill aquifer. All of the sampled wells are also equipped with pressure transducers that measure the water level every five minutes – these data were downloaded every time the well was sampled.

We began sampling from each well by measuring the depth to water and total well depth with an electric tape. We then purged the well by bailing out twice the volume of water that was initially in it to ensure that the water we ultimately collected was truly representative of the aquifer. After purging, we used the bailer to bring up water and emptied it into two separate beakers using a bottom-emptying device which limits atmospheric disturbance to the water during removal from the bailer. We submerged field probes into one of the beakers of groundwater for temperature, pH, conductivity, and dissolved oxygen measurements, and

syringe-filtered the water from the other beaker in the same manner as described for the stream samples. The 4-6 Lower Eiss well often did not yield enough water for the full suite of geochemical analyses – in these cases, we only collected enough water from this well for major ion analysis. Some of the analysis in this study incorporates N4D groundwater chemistry and water elevation data from Andrews (2021) which was collected following the same methodology as described above.

2.3 Laboratory Methods

We conducted most geochemical analyses at Dr. Matthew Kirk's Aqueous Geochemistry Lab at Kansas State University. We measured alkalinity in all surface and groundwater samples using the Gran alkalinity titration method with 0.02 N H_2SO_4 as the titrant. We measured major ion concentrations (Na^+, NH_4^+, K^+, Mg^{2+}, Ca^{2+}, Sr^{2+}, F^-, Cl^-, NO^{2-}, Br^-, NO_3^-, and SO_4^{2-}) using a Thermo Scientific ICS-1100 Ion Chromatograph (IC) and non-purgeable organic carbon (NPOC) and total dissolved nitrogen (TN) using a Shimadzu TOC-L. We sent surface, groundwater, and precipitation samples to the Stable Isotope Mass Spectrometry Laboratory at the Kansas State University Division of Biology to measure the $\delta^{18}O$ and δD of water. Results are presented as per mil (‰) relative to Vienna Standard Mean Ocean Water (VSMOW). We analyzed all samples within a month of collection.

2.4 Calculations and Analysis

2.4.1 Concentration-Discharge

We evaluated concentration-discharge (C-Q) relationships for major ions in the stream water to better understand water flow paths at N4D. C-Q analysis provides a quantitative description of the solute export behavior of a catchment, which can be useful for making inferences about the water flow paths that transport the solutes (e.g. Godsey et al., 2009; Sullivan

et al., 2019; Stewart et al., 2022). Broadly speaking, each solute can be classified as either chemodynamic or chemostatic depending on whether its concentration in the stream water changes with stream discharge. Solutes that display chemostatic behavior have relatively constant concentrations in the face of large fluctuations in discharge, and this behavior usually arises because the catchment area contains large surplus storages of these solutes. Examples of solutes that are typically chemostatic are mineral weathering products like Ca^{2+}, Mg^{2+}, and SiO_2^{2-}, and, in the case of agricultural catchments, fertilizer products like total nitrogen and phosphorus. Chemodynamic solutes, on the other hand, have their concentrations fluctuate along with discharge. Chemodynamic behavior is further divided into mobilization behavior, where an increase in discharge results in a higher concentration of the solute, and dilution behavior, where an increase in discharge results in a lower concentration of the solute. These behaviors can arise when a solute is limited in quantity, distributed unequally throughout the catchment area, or variably connected to the stream depending on flow conditions (Musolff et al., 2015).

There are two primary ways of quantifying the C-Q behavior of a solute. The first is to calculate the 'b' parameter in the power law relationship $C = aQ^b$, where C is solute concentration, Q is discharge, and a and b are fitting parameters derived from the regression. The b parameter is simply the slope of the best fit line when concentration and discharge are plotted on a log-log chart, so a low slope ($b \approx 0$) implies mostly chemostatic behavior while higher slopes ($b \neq 0$) imply progressively more chemodynamic behavior. Chemodynamic solutes with a positive slope ($b > 0$) are displaying mobilization behavior while those with a negative slope ($b < 0$) are displaying dilution behavior (Godsey et al., 2009). While this method provides information on the type and strength of C-Q behavior, it is somewhat flawed in that it does not inform on the actual concentration variability of the solute in question. A solute could

have considerable variation in its concentration through time but still be labeled as chemostatic through this method ($b \approx 0$) if the concentration does not strongly correlate with discharge in a certain direction (Thompson et al., 2011).

The second method for quantifying C-Q behavior addresses this flaw by centering on concentration variability. This method is to calculate the ratio of the coefficients of variation (CV) between the solute and discharge:

$$\frac{CV_C}{CV_Q} = \frac{\frac{\sigma_C}{\mu_C}}{\frac{\sigma_Q}{\mu_Q}} = \frac{\sigma_C}{\sigma_Q}\frac{\mu_Q}{\mu_C}$$

where σ is the standard deviation and μ is the mean of solute concentration (subscript C) and stream discharge (subscript Q). From this equation, chemostatic behavior is defined by low variability in concentration relative to discharge (i.e. $\frac{CV_C}{CV_Q} \approx 0$) while increasingly positive values of $\frac{CV_C}{CV_Q}$ imply increasingly chemodynamic behavior. This method can correctly classify solutes with highly variable concentrations as chemodynamic, but by design it does not incorporate any potential direction in the relationship between concentration and discharge (Thompson et al., 2011).

C-Q studies often combine the two methods to provide a holistic view of a catchment's solute export behavior. A common way to show the results of both methods is a chart with $\frac{CV_C}{CV_Q}$ and b for each measured solute on the x- and y-axis, respectively (Figure 6) (e.g. Musolff et al., 2015; Sullivan et al., 2019). In such a chart, chemostatic solutes plot near the origin ($\frac{CV_C}{CV_Q}$, $b \approx 0$) while chemodynamic solutes will plot with $\frac{CV_C}{CV_Q} > 0$ and b-values in different positions depending on the specific behavior of the solute. Mobilizing solutes will have $b > 0$, diluting solutes will

have b < 0, and solutes that are highly variable but do not correlate strongly with discharge will plot somewhere close to the x-axis ($\frac{CV_C}{CV_Q} > 0$, b ≈ 0). By simultaneously communicating the concentration variability and correlation to discharge of each solute, these charts provide a quick way to assess overall export behavior in the catchment. Solutes that plot closely together are likely subject to the same transport processes, and chemodynamic solutes that do not plot within the typical mobilization/dilution zones are likely subject to complex processes that bear further consideration.

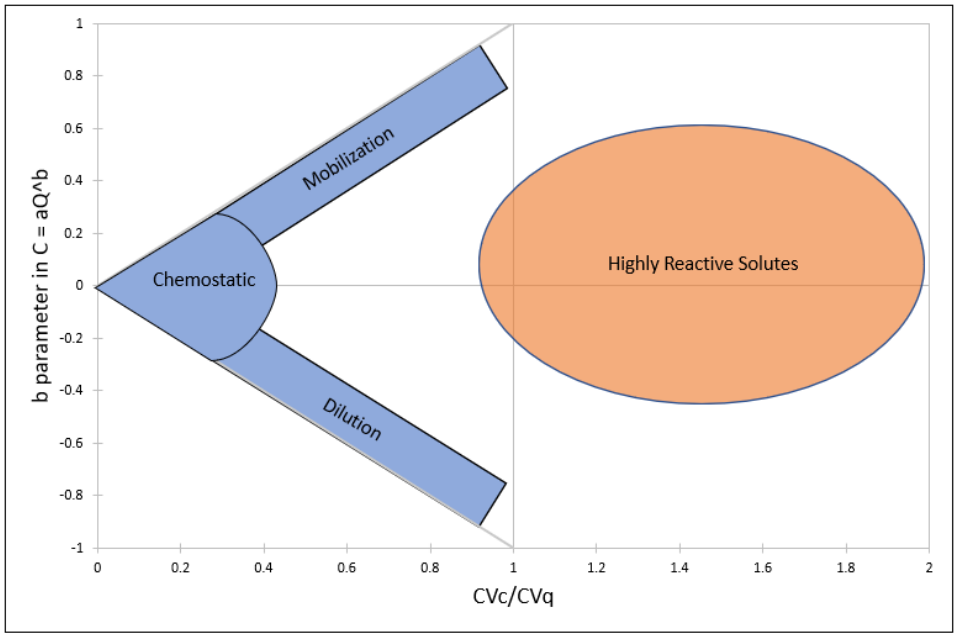

Figure 6. Conceptual diagram of a C-Q analysis summary chart. The ratio of coefficients of variation is on the x-axis and the slope of the power law relationship between concentration and discharge is on the y-axis. The chart area is broken up into zones describing the general transport behaviors of solutes that plot within them.

In this study, we applied C-Q analysis to the major ion concentrations measured by IC. Every stream sample was matched up to its closest discharge value from the stream gauge at the catchment outlet. We plotted the concentrations of every major ion in each stream sample against the corresponding discharge value to acquire each ion's *b* parameter, and then calculated coefficients of variation for the ions and discharge to acquire $\frac{CV_C}{CV_Q}$. We used the results of this

analysis to qualitatively group ions into transport regimes and draw conclusions about streamflow generation based on solute export behavior.

2.4.2 Endmember Mixing

The second analysis that we performed for this study was endmember mixing analysis. Mixing analysis is a core component of many studies on streamflow generation (e.g. Liu et al., 2004; Cowie et al., 2017; Dwivedi et al., 2019) because it allows for a quantitative assessment of the contribution to streamflow from any number of potential water sources using only water chemistry data. The central concept of mixing analysis is that whenever two water sources mix, the concentration of a tracer solute in the mixed water will equal the average concentration in the sources weighted by their fractional contributions to the mix:

$$X_M = X_A f_A + X_B f_B$$

where X is the concentration of any given solute, f is a source's fractional contribution to the mix, and subscripts M, A, and B denote the mixed water and two water sources A and B, respectively. Adding a second condition – that the fractional contributions of the two sources add to 1 – allows for a direct calculation of a source's fractional contribution from solute concentrations:

$$f_A + f_B = 1$$

$$f_A = \frac{X_M - X_B}{X_A - X_B}.$$

The above relationships can be expanded to include more than two contributing water sources, but each additional source requires the addition of another tracer and an increasingly complex system of equations. For instance, fractional contributions from three endmembers (A, B and C) can be calculated with concentrations from two tracers (X and Y) using the following equations:

$$X_M = X_A f_A + X_B f_B + X_C f_C$$

$$Y_M = Y_A f_A + Y_B f_B + Y_C f_C$$

$$f_A + f_B + f_C = 1$$

which can be rearranged into the solvable system:

$$f_A = \frac{Y_M - Y_B + Y_B f_C - Y_c f_C}{Y_A - Y_B}$$

$$f_B = \frac{X_M - X_A + X_A f_C - X_C f_C}{X_B - X_A}$$

$$f_C = 1 - f_A - f_B.$$

Mixing analyses can be further expanded to *n* endmembers, but principal component analysis (PCA) is generally required to handle the mathematical complexity that comes with the addition of more tracers (Christophersen and Hooper, 1992).

Selecting which endmembers and tracers to use is the key consideration when employing mixing analysis. While endmembers can be statistically determined from the stream chemistry data alone (Christophersen and Hooper, 1992), they can also be chosen ahead of time based on previous understanding of the system in question (Inamdar, 2011). In N4D, we assumed that the stream water is composed of precipitation, soil water, and multiple groundwater endmembers based on the work of Sullivan et al. (2019). We selected tracers based on which solutes showed the most variation between these endmembers while having minimal variation within each endmember. We then verified the final selection of endmembers and tracers by plotting the tracer averages for each endmember on a bivariate plot and ensuring that they completely bounded all stream samples. After verification, we applied the above mixing calculations in order to elucidate the fractional contribution of each water source to streamflow.

Because there ended up being more than three endmembers to consider, we first used isotope hydrograph separation (IHS) to calculate the fractional contribution from precipitation separately. From this, we could account for the influence of precipitation on the stream chemistry at every sampling point and simplify the calculations for the remaining endmembers. IHS uses the same principles and equations as the generalized mixing analysis detailed above but refers to the specific application of the stable water isotopes $\delta^{18}O$ and δD as tracers for separating meteoric water from baseflow during storms (Klaus and McDonnell, 2013). In principle, baseflow (often referred to as pre-event water in IHS contexts) has different isotopic compositions from meteoric water (referred to as event water) because it has existed on the surface for an extended period of time and been subjected to processes that alter isotopic ratios like evaporation and water-rock interaction. IHS is useful for hydrologic analysis because it can reveal how dominant runoff processes are in a catchment based on the calculated proportions of event water to pre-event water through the course of a storm and its aftermath (Figure 7) (e.g. Hangen et al., 2001; Liu et al., 2004).

In this study, we perform IHS to calculate the fractional contribution of precipitation to the stream water throughout the study period. We apply mixing calculations to each stream water sample using $\delta^{18}O$ and δD VSMOW values as tracers. $\delta^{18}O$ and δD values from the most recently collected precipitation sample comprise the event endmember, and $\delta^{18}O$ and δD values from the most recent groundwater sampling event, averaged across all groundwater sources, comprise the pre-event endmember. By first applying IHS to each stream sample, we separately account for the contribution from precipitation and then dissect the pre-event component into its various subsurface sources with the relatively simple three endmember mixing calculations.

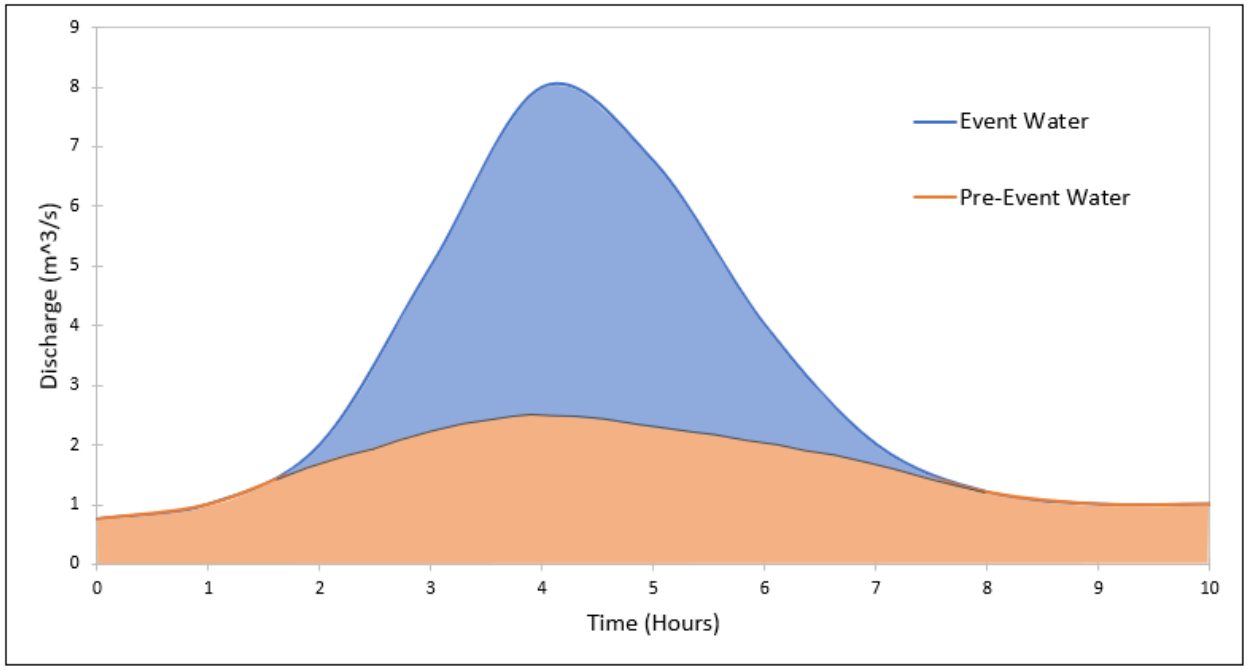

Figure 7. Conceptual diagram of a hydrograph that has been separated into event water and pre-event water components through isotope hydrograph separation. The dominance of runoff in a catchment is represented by the extent that the event water curve rises above the pre-event water curve.

2.4.3 Groundwater Head Gradients

In order to help explain any shifts in the groundwater contributions to streamflow, we analyzed the water elevation data from the pressure transducers in five of the N4D groundwater monitoring wells. While the Lower Eiss and Upper Eiss aquifers each only have one well equipped with a pressure transducer, the Morrill aquifer has three (Figure 8). With three points of elevation data, we could calculate the geometry of the water table between those points using typical three-point problem calculations (e.g. Fienen, 2005). Each pressure transducer records water elevation every five minutes, so we matched up data points between the three Morrill wells and calculated the gradient and gradient direction of the water table for each time point. We did these calculations for all time points within the study period as well as time points going back to 2/27/2020 in order to investigate water table trends in different seasons.

Figure 8. Locations of the three Morrill limestone wells equipped with pressure transducers. Yellow pins denote the well location and blue lines between each well are labelled with distance in meters. Using the spatial positioning of these wells and the elevation of water within them at any given time, we calculated the gradient and direction of groundwater flow in the immediate vicinity of this triangle.

Chapter 3 - Results

3.1 Sampling Period Precipitation and Discharge

Figure 9 shows daily total precipitation and average discharge for N4D in 2021. The catchment received 620.5 mm of rain over the whole year, which is 74.3% of the annual average (Hayden, 1998). 353.9 mm of precipitation fell within the sampling period (4/15/ – 7/16), which is 57% of the total precipitation for the year. The precipitation regime is dominated by short, intense storms rather than drawn out periods of continuous precipitation and indeed, 49.9% of precipitation that fell within the sampling period is accounted for by just two storms (5/16 and 7/15).

The flume at the outlet of the catchment recorded discharge for most of the sampling period, with the exception of a dry period between 7/5 and 7/14. Flow was modest at the beginning of the sampling period, averaging 0.004 m^3/s between 4/15 and 5/15 as the stream was fed by spring precipitation. The large storm on 5/16 caused discharge to spike to its maximum for the year of 4.69 m^3/s, which then dropped to an average of 0.077 m^3/s on the following day. Discharge generally decreased over the remainder of the sampling period and dried out completely on 7/5. Over this drying period, occasional storms brought small spikes in discharge, including the large storm on 7/15 which caused a week-long return of modest flow over the flume after it had been completely dry. Across the whole sampling period, 1.49×10^5 m^3 of water exited N4D via the stream. This equates to 109.9 mm of water thickness over the whole catchment, which is 31% of the sampling period precipitation.

The storms that we selected for hourly sampling covered a range of conditions and are marked in Figure 9 along with their key hydrologic characteristics. Total precipitation that fell for these events ranged from 2.80 mm to 80.0 mm and their spacing throughout the sampling

period meant that they covered a variety of antecedent flow conditions. One event coincided with the low-flow period before the large 5/16 storm, three events occurred over the progressive drying period after the 5/16 storm, and one event covered the large 7/15 storm that produced flow after the prolonged dry period.

3.2 Water Chemistry

Figures 11 and 12 summarize the chemical parameters and major ion concentrations of the surface and groundwater that we collected in this study. Over the course of the sampling period, we collected 44 stream samples and six samples from each of the three wells at the 4-6 nest site: 4-6 Mor (Morrill limestone), 4-6 Eis 1 (Lower Eiss limestone), and 4-6 Eis 2 (Upper Eiss limestone). We supplemented our groundwater data with nine samples from 4-6 Mor, eight samples from both 4-6 Eis 1 and 4-6 Eis 2, and 10 samples from both 3-5 Mor and 3-5-1 Mor that were collected between 6/25/2020 and the beginning of this study, previously published in Andrews (2021). For both surface and groundwater samples, the concentrations of NO_2^-, NO_3^-, Br^-, NH_4^+, TN, and NPOC were frequently below the detection limits of our methods and thus excluded from the remainder of the analysis. The full data are tabulated in Appendix A.

Compared to the groundwater samples, the stream water samples we collected tended to have higher pH and lower alkalinity content and specific conductivity. pH, alkalinity content, and specific conductivity are similar across groundwater samples from each well. Dissolved oxygen measured in the stream shows significant variation, ranging from 1.9 to 9.8 mg/L, with an average of 7.91 mg/L. Groundwater samples have similar dissolved oxygen concentrations typically ranging from 4.4 to 7.6 mg/L in all wells except 3-5-1 Mor. 3-5-1 Mor is the deepest well and has an average dissolved oxygen concentration of 2.69 mg/L.

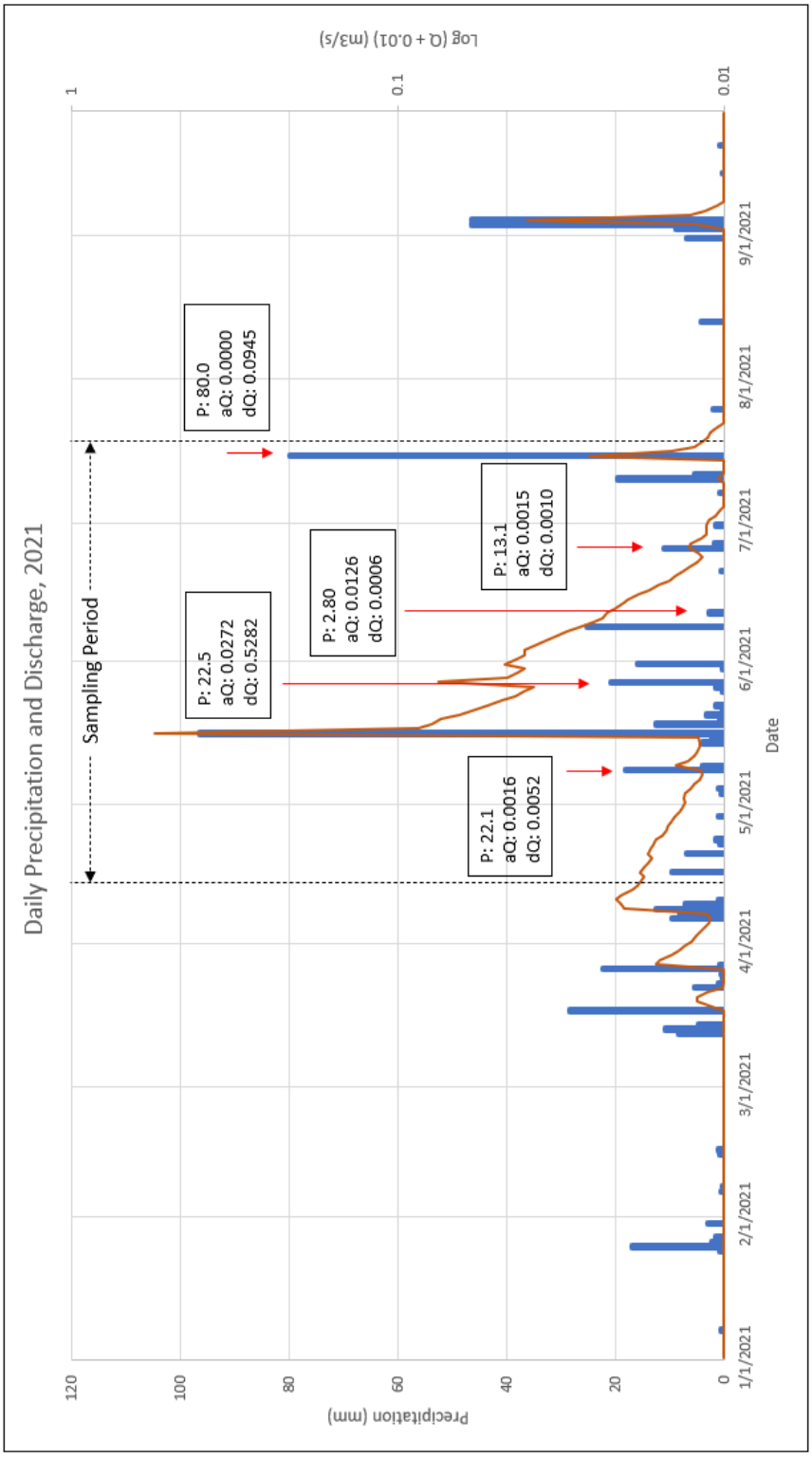

Figure 9. Daily total precipitation (blue bars) and average discharge (orange line) in N4D for 2021. 0.01 was added to each discharge value so that no-flow days could be displayed on a log scale. Sampling period is outlined by dashed lines and hourly-sampled storms are marked with red arrows. Total precipitation (P), antecedent discharge (aQ), and the difference between maximum discharge and antecedent discharge (dQ) is provided for each marked storm.

The most abundant major ions in all water sources are Ca^{2+}, Mg^{2+}, and SO_4^{2-}. The range of Ca^{2+} concentrations in the stream water overlaps with the ranges of all other sources, with a lowest source average of 77.1 mg/L in 4-6 Eis 1 and a highest source average 101.2 mg/L in 3-5 Mor. The average Ca^{2+} concentration in stream water falls in the lower end of this range at 83.0 mg/L. Mg^{2+}, on the other hand, shows more significant variation between sources. The range of Mg^{2+} concentrations in the stream water does not overlap at all with the ranges of 3-5-1 Mor or 4-6 Eis 1, which are significantly higher (stream average 15.6 mg/L, 3-5-1 Mor average 28.9 mg/L, 4-6 Eis 1 average 25.2 mg/L). While the other groundwater samples do overlap with the stream water's range, the averages in 3-5 Mor and 4-6 Mor are higher than the stream water's maximum. Only 4-6 Eis 2 has an average Mg^{2+} concentration (14.1 mg/L) which lies in the stream water's range. The stream water has its widest variation in SO_4^{2-} concentration, ranging from 12.9 mg/L to 34.0 mg/L with an interquartile range of 16.2 mg/L. This range is bracketed by the average SO_4^{2-} concentrations of 4-6 Eis 2 (11.3 mg/L) and 3-5-1 Mor (41.9 mg/L).

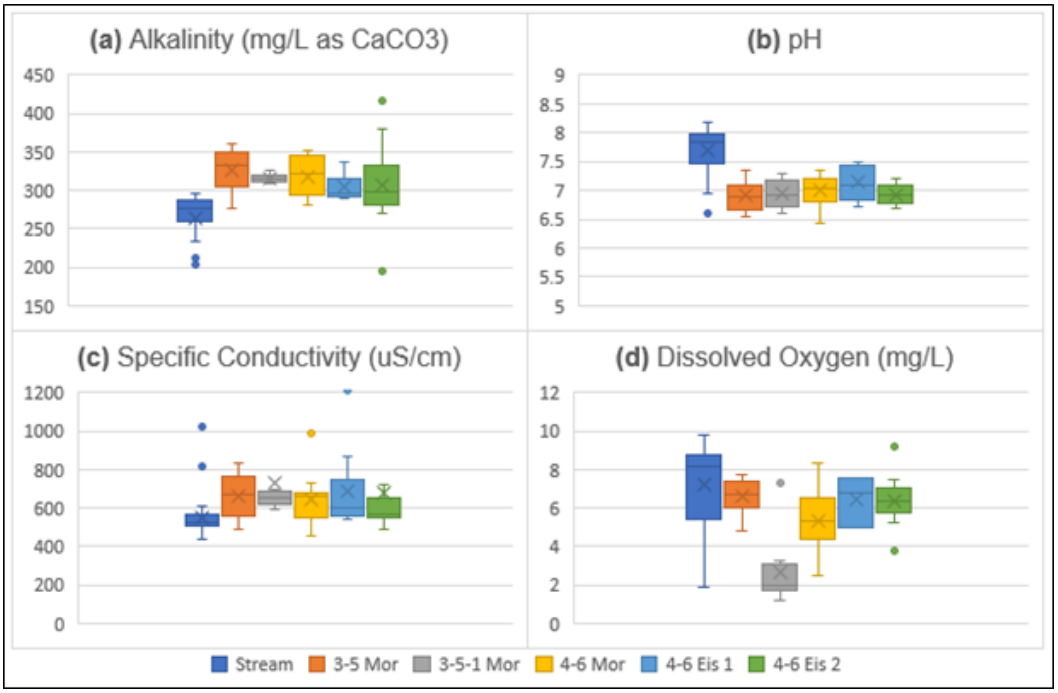

Figure 10. Box plots of alkalinity (a), pH (b), specific conductivity (c), and dissolved oxygen concentrations (d) in all surface and groundwater samples. X's mark means and dots mark outlier points.

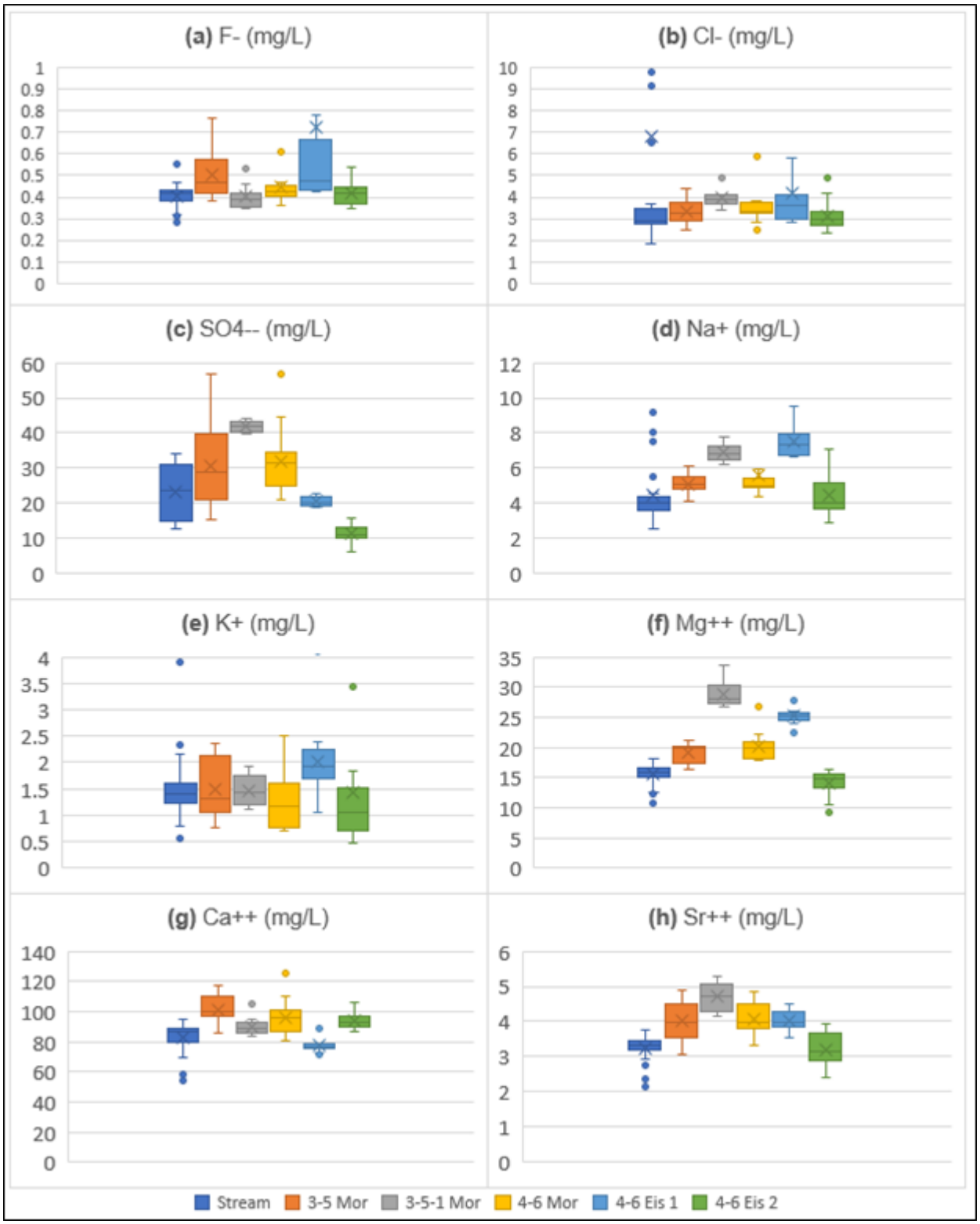

Figure 11. Box plots of fluoride (a), chloride (b), sulfate (c), sodium (d), potassium (e), magnesium (f), calcium (g), and strontium (h) concentrations in all surface and groundwater samples. X's mark means and dots mark outlier points.

Some samples of the stream water contained Cl^-, Na^+, and K^+ concentrations that are 3 – 50 times higher than the median. The highest of these outlier points were not included in the box plots in Figure 11 for ease of reading but are shown in Figure 12 within time series plots of concentration over the entire sampling period. The extreme outlier points for all three of these ions occur on 5/8 – 5/9, which coincides with the first storm that we sampled hourly. This was also the first major rain event to occur after N4D was burned on 4/12.

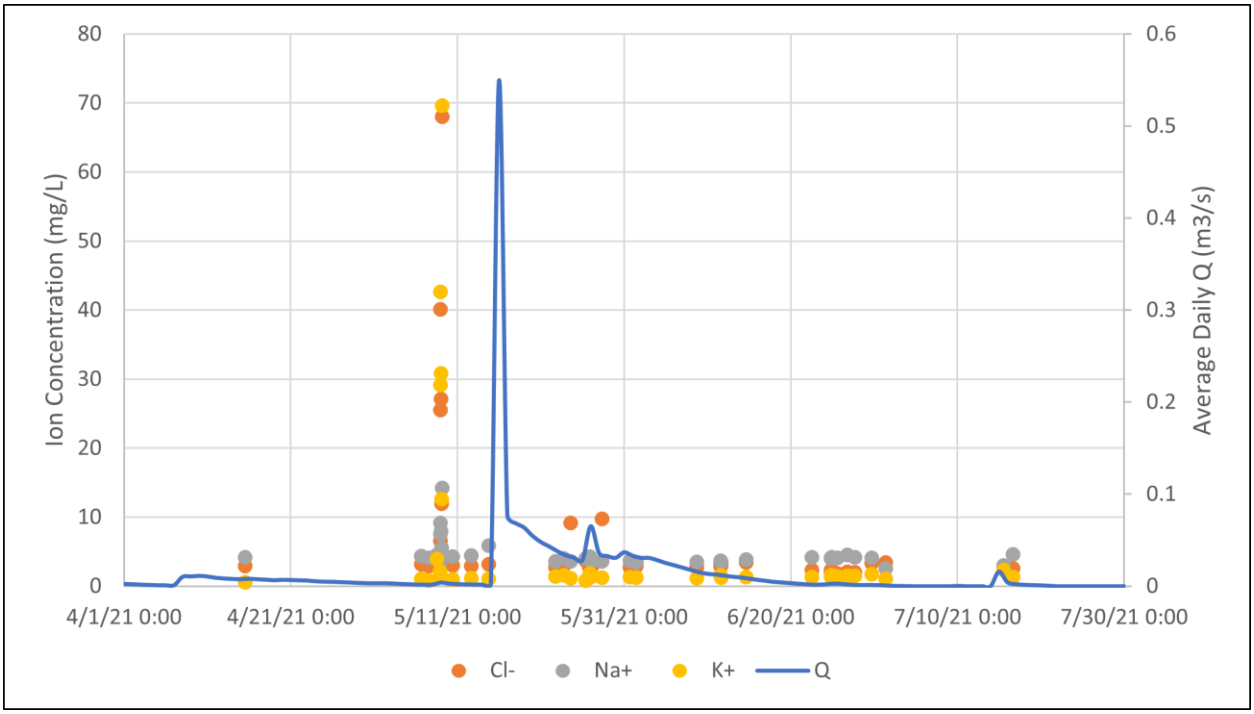

Figure 12. Time series plot of chloride, sodium, and potassium concentrations in the stream over the entire sampling period. Average daily discharge in the stream is provided for reference.

3.3 Stable Water Isotopes

Figure 13 shows the stable water isotope ratios in all of the samples we collected for this study. Of the 44 total stream water samples, we analyzed 42 for $\delta^{18}O$ and δD VSMOW. We also analyzed five samples from both 4-6 Mor and 4-6 Eis 2, and four samples from 4-6 Eis 1. Groundwater from 3-5 Mor and 3-5-1 Mor was not collected for isotope analysis. During three of the hourly-sampled storms we collected enough rainwater for duplicate water isotope analyses, and during the other two storms we

only collected enough for a single analysis, for a total of eight precipitation samples. For validation, we also include stable water isotope data from a National Ecological Observatory Network (NEON) site at Kings Creek, just downstream of N4D (NEON, 2022). The NEON data samples we use were collected between April and July in 2020 and 2021. The full isotope data are tabulated in Appendix A.

The local meteoric water line (LMWL) shown in Figure 13 was calculated from precipitation water isotopes collected at Konza over the last 20 years and is defined by the line $\delta D = 7.4038*\delta^{18}O + 2.353$ (personal communication, Dr. Jesse Nippert). A linear regression line fits to the data that we collected plus the NEON data and is defined by $\delta D = 7.1422*\delta^{18}O + 4.9296$. The samples fit closely to this line with $R^2 = 0.9662$. In general, the $\delta^{18}O$ and δD values of the stream water samples lie in between those of the groundwater and those of the precipitation samples. Stream water ranges in $\delta^{18}O$ between -5.7 and -4.5‰, while groundwater ranges between -6.2 and -5.3‰ and precipitation between -4.4 and 0‰. NEON samples from Kings Creek collected in April – June have lower $\delta^{18}O$ and δD values than those collected in July.

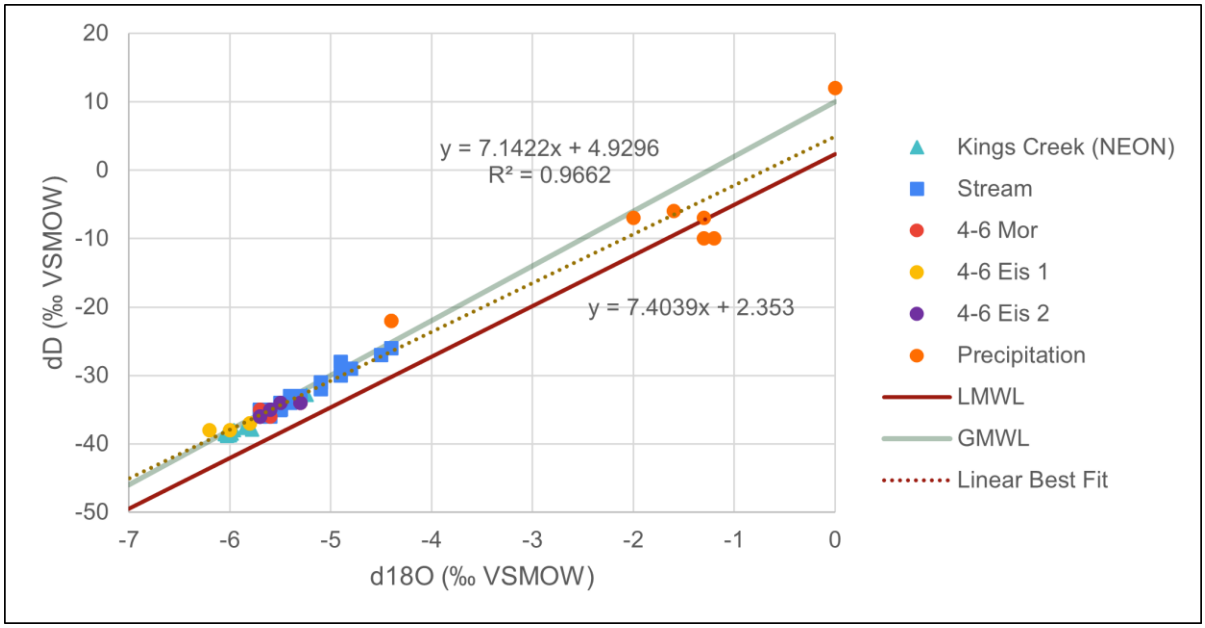

Figure 13. Stable water isotopes in stream water, groundwater, and precipitation at N4D as well as surface water at Kings Creek via NEON. Solid line denotes the local meteoric water line calculated from historical isotope ratios (personal communication, Dr. Jesse Nipper), the dashed line denotes the linear regression of all plotted samples, and the faded line denotes the Global Meteoric Water Line.

3.4 Concentration-Discharge Analysis

Figure 14a shows a plot of *b* vs $\frac{CV_C}{CV_Q}$ for each solute. Because of the large impact that the anomalously high Cl^-, Na^+, and K^+ concentrations on 5/8-5/9 have on C-Q calculations, we also show C-Q results with all samples from 5/8-5/9 removed in Figure 14b. A table of *b* and $\frac{CV_C}{CV_Q}$ values is provided in Appendix B.

In the data set with the 5/8-5/9 samples included, all solutes plot near the origin except for Cl^-, Na^+, K^+, and SO_4^{2-}. Cl^-, Na^+, and K^+ all have large $\frac{CV_C}{CV_Q}$ values (1.58, 0.39, 2.15, respectively), but plot close to the x-axis with low-magnitude *b* parameters (-0.01, -0.06, -0.11, respectively). SO_4^{2-} has a moderately high $\frac{CV_C}{CV_Q}$ of 0.30 but also the highest-magnitude *b* parameter of -0.26. With the 5/8-5/9 samples removed, Cl^-, Na^+, and K^+ all move closer to the origin with decreased $\frac{CV_C}{CV_Q}$ values of 0.52, 0.14, and 0.23, respectively. The *b* parameter of Cl^- moves to a moderately positive value of 0.09. SO_4^{2-} remains in roughly the same position with $\frac{CV_C}{CV_Q}$ = 0.37 and *b* = -0.26.

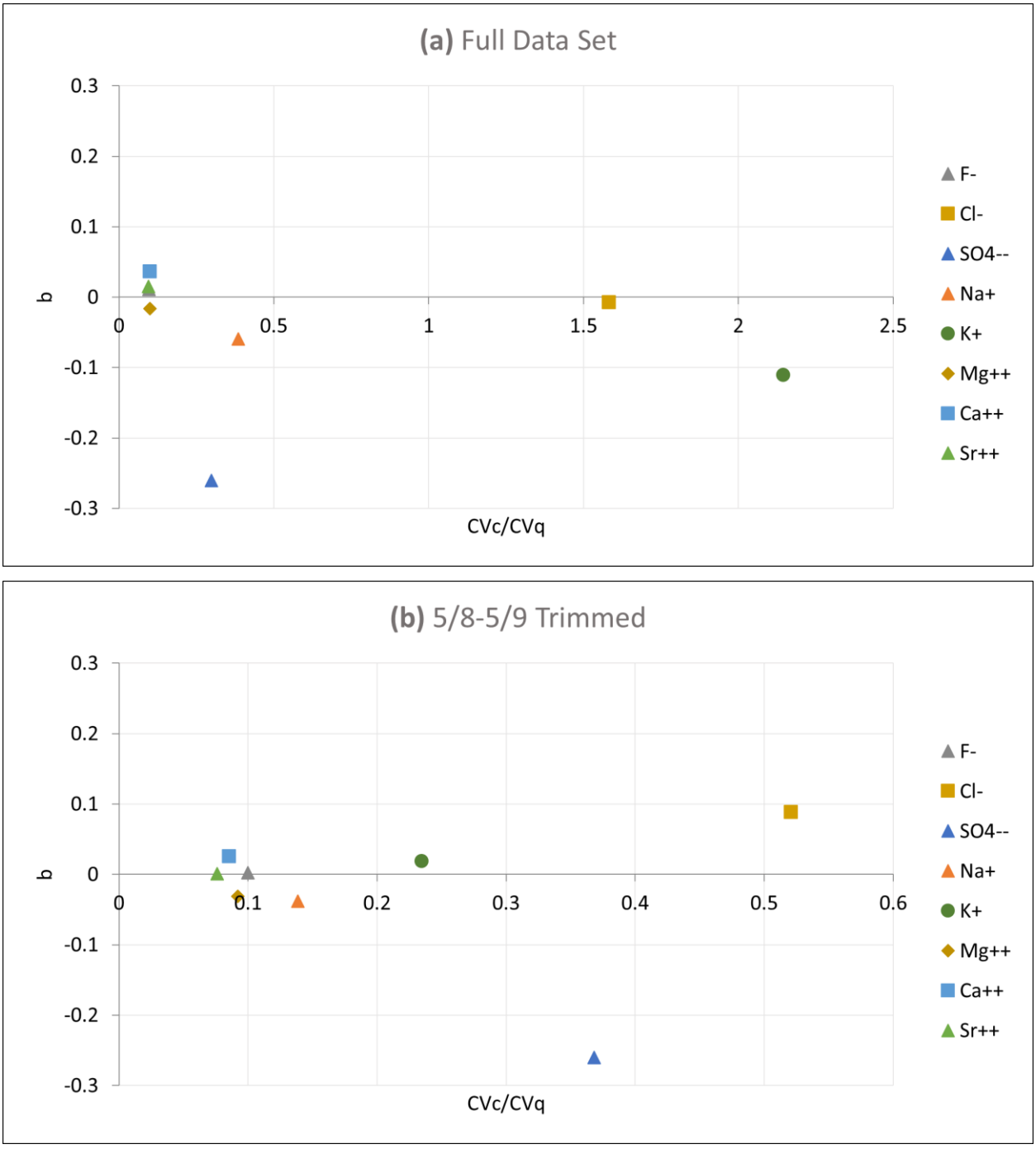

Figure 14. *b* vs. $\frac{CV_C}{CV_Q}$ plots of stream water solutes for the full data set (a) and a data set with 5/8 – 5/9 samples removed (b). Note differences in x-axis scaling.

4.5 Mixing Analysis

4.5.1 Isotope Hydrograph Separation

Figure 15 shows the fractional contributions of event water (precipitation, runoff) and pre-event water (groundwater, soil water) to each stream sample through the sampling period based on the average of two two-endmember mixing calculations using $\delta^{18}O$ and δD as tracers. The $\delta^{18}O$ and δD values used as the endmember compositions varied with each storm, with the event endmember compositions coming from the most recent precipitation sample and the pre-event endmember compositions coming from an average of the most recent groundwater samples from each well. The three stream water samples that were collected before any precipitation in the sampling period (4/15, 5/6, and 5/7) are excluded from calculations and assumed to have no contribution from event water. The endmember compositions used for each range of dates are provided in Table 1. Fractions of event water in each water sample are tabulated along with water chemistry in Appendix A.

Table 1. Stable water isotope ratios used for endmember mixing between event and pre-event water. All isotope ratios are in units of ‰ VSMOW.

Date Range		Event Endmember		Pre-event Endmember	
Start	End	$\delta^{18}O$	δD	$\delta^{18}O$	δD
5/6	5/14	-1.8	-6.5	-5.7	-36
5/22	6/1	-1.25	-10	-5.7	-35
6/8	6/14	0	12	-5.6	-35
6/22	6/27	-1.3	-7	-5.6	-35
7/15	7/16	-4.4	-22	-5.6	-36

Fractional contribution of event water increases during storms, but the magnitude of the increase varies significantly. Table 2 summarizes the hydrologic characteristics of each hourly-sampled storm along with the maximum fraction of event water (fQ_e) and the maximum

discharge of event water ($Q_e = fQ_e * Q_{stream}$) that the stream reaches during each storm. The largest fQ_e of 0.577 occurs in the immediate aftermath of the storm on 7/15, which happened after a prolonged dry period and was also the sampled storm with the highest amount of precipitation. Two storms (5/8-5/9 and 5/26-5/26) had very similar amounts of precipitation (22.1 and 22.5 mm) but significantly different values of fQ_e (0.336 and 0.074). The difference between these storms was the flow conditions in the stream prior to precipitation – in the 5/8-5/9 storm, the stream was nearly dry with a discharge of 0.0016 m^3/s and in the 5/26-5/27 storm flow was over an order of magnitude larger with a discharge of 0.0272 m^3/s. The smallest storm, 6/11, only had 2.80 mm of precipitation and resulted in an insignificant amount of event water in the stream ($fQ_e = 0.009$).

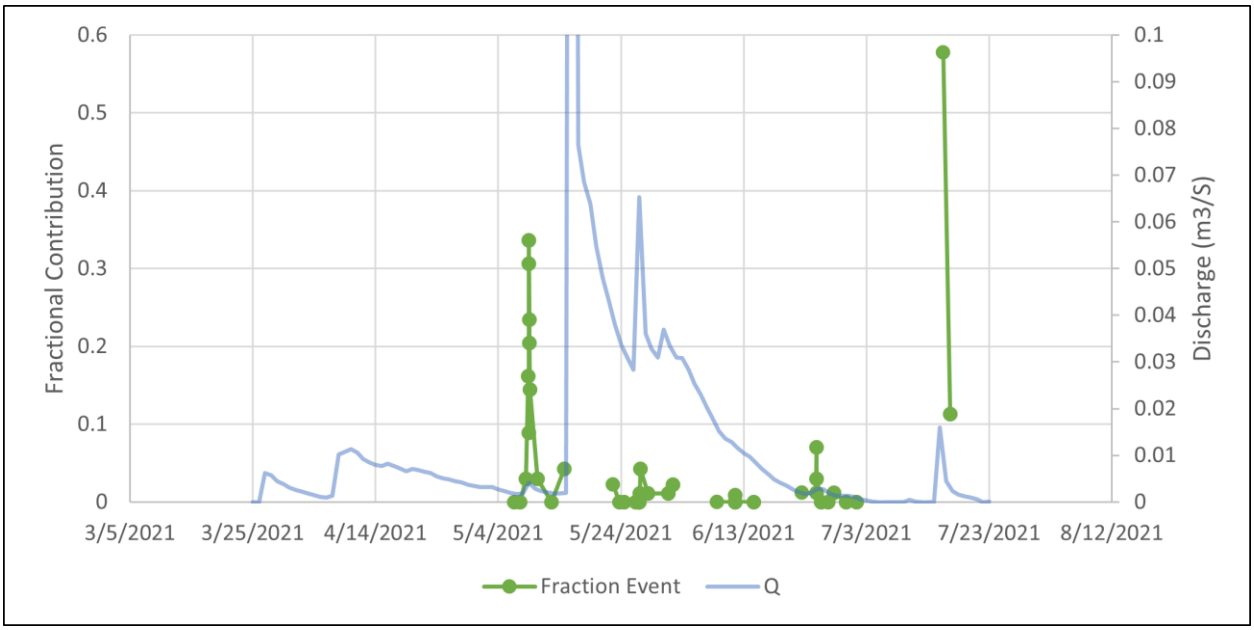

Figure 15. Fractional contribution of event water in the stream during the sampling period. Stream discharge is marked with the blue line for reference of flow conditions. Gaps between data points indicate long periods of time without sampling and a changes to the endmember isotope ratios used in mixing calculations.

Table 2. Hydrologic characteristics for each hourly-sampled storm. fQ_e is the maximum fraction of event water attained in the storm, Q_e is the maximum flow rate of event water in the attained in the storm, P is precipitation amount, aQ is discharge in the stream prior to the storm, and dQ is the maximum change in discharge that occurs as a result of the storm.

Date	fQ_e	Q_e (m^3/s)	P (mm)	aQ (m^3/s)	dQ (m^3/s)
5/8-5/9	0.336	0.0019	22.1	0.0016	0.0052
5/26-5/27	0.074	0.0031	22.5	0.0272	0.5282
6/11	0.009	0.0001	2.80	0.0126	0.0006
6/24-6/25	0.071	0.0001	13.1	0.0015	0.0010
7/15	0.577	0.0102	80.0	0.0000	0.0945

4.5.2 Three-Endmember Mixing

We used the concentration of SO_4^{2-} and the concentration ratio Ca^{2+}/Mg^{2+} as the tracers for further mixing analyses. Both tracers met our criteria laid out in the methods section of having high variation between endmembers but low variation within endmembers. Figure 16 shows that the values of these tracers in potential endmembers bracket the values of these parameters in the stream water, and excluding outliers, these tracers plot in a single cluster for each potential endmember. Figure 16 includes compositions of multiple water sources that potentially contribute to streamflow: groundwater from the three limestone aquifers in the lower portion of N4D collected from five wells, soil water reported by Tsypin and Macpherson (2012), and precipitation collected and averaged over 30 years (Blair, 2019).

Figure 17 shows our endmember selection and the resulting mixing envelope. Of the potential groundwater sources, water within the 3-5 Mor and 4-6 Mor wells is likely to have already been mixed with stream water (Macpherson, 1996; Barry, 2018), making these unsuitable endmembers for stream water mixing calculation. The Lower Eiss aquifer (represented by 4-6 Eis 1) has a much lower hydraulic conductivity than the other aquifers and

has been shown to have little interaction with the stream (Pomes, 1995; Macpherson, 1996), so we also excluded it as an endmember. We already accounted for the contribution of precipitation using mixing calculations with stable isotope ratios (Figure 15), so we adjusted the SO_4^{2+} and Ca^{2+}/Mg^{2+} values for each stream sample to remove the chemical influence of precipitation according to the sample's fraction of event water. This resulted in a slight rightwards shift in stream data points between Figures 17 and 18. Thus, 3-5-1 Mor, 4-6 Eis 2, and the soil water values from Tsypin and Macpherson (2012) are left as the last three likely endmembers that fully enclose the stream water data points.

Figure 18 shows the results of three-endmember mixing calculations using the average values of SO_4^{2+} and Ca^{2+}/Mg^{2+} in 3-5-1 Mor, 4-6 Eis 2, and soil water. Soil water input to the stream is very low throughout the sampling period with an average fractional contribution of 0.005 and a maximum of 0.028. Water from 4-6 Eis 2 dominates streamflow for much of the sampling period with an average fractional contribution of 0.617 and a range of 0.313 – 0.831. Fractional contribution from 3-5-1 Mor is slightly lower, with an average of 0.321 and a range of 0.097 – 0.590. 4-6 Eis 2 reaches its maximum contribution during the high flow conditions after the large storm on 5/16 and is slowly overtaken by 3-5-1 Mor over the following weeks as discharge in the stream decreases. 3-5-1 Mor overtakes 4-6 Eis 2 on 6/24 and reaches its maximum contribution on 6/27, when discharge in the stream fell to 0.001 m^3/s. During the sampled storms that produced a high fractional input of event water, the fractional contributions of both groundwater sources decrease substantially, but the fractional contribution of soil water stays relatively constant. The fractional contributions from each source are tabulated for each stream water sample in Appendix A.

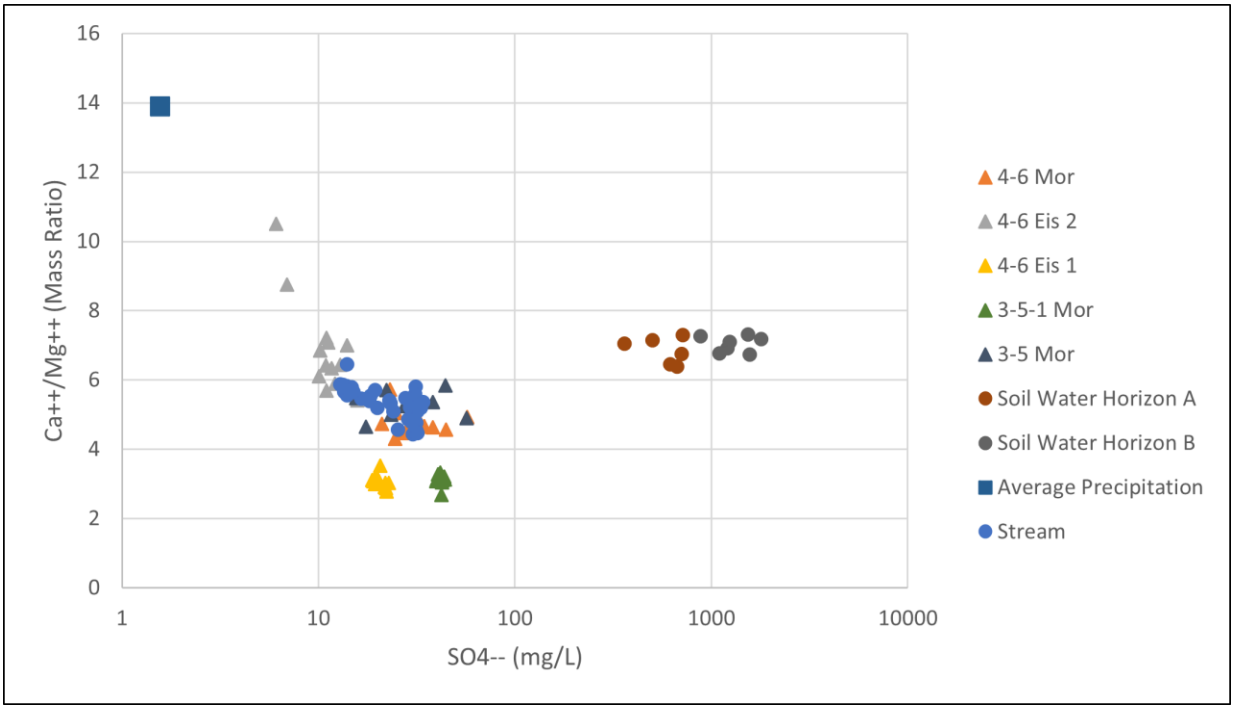

Figure 16. Bivariate plot of Ca^{2+}/Mg^{2+} vs. SO_4^{2-} for stream water samples and the various potential endmembers. Stream samples are denoted with blue circles and groundwater sources are denoted with triangles.

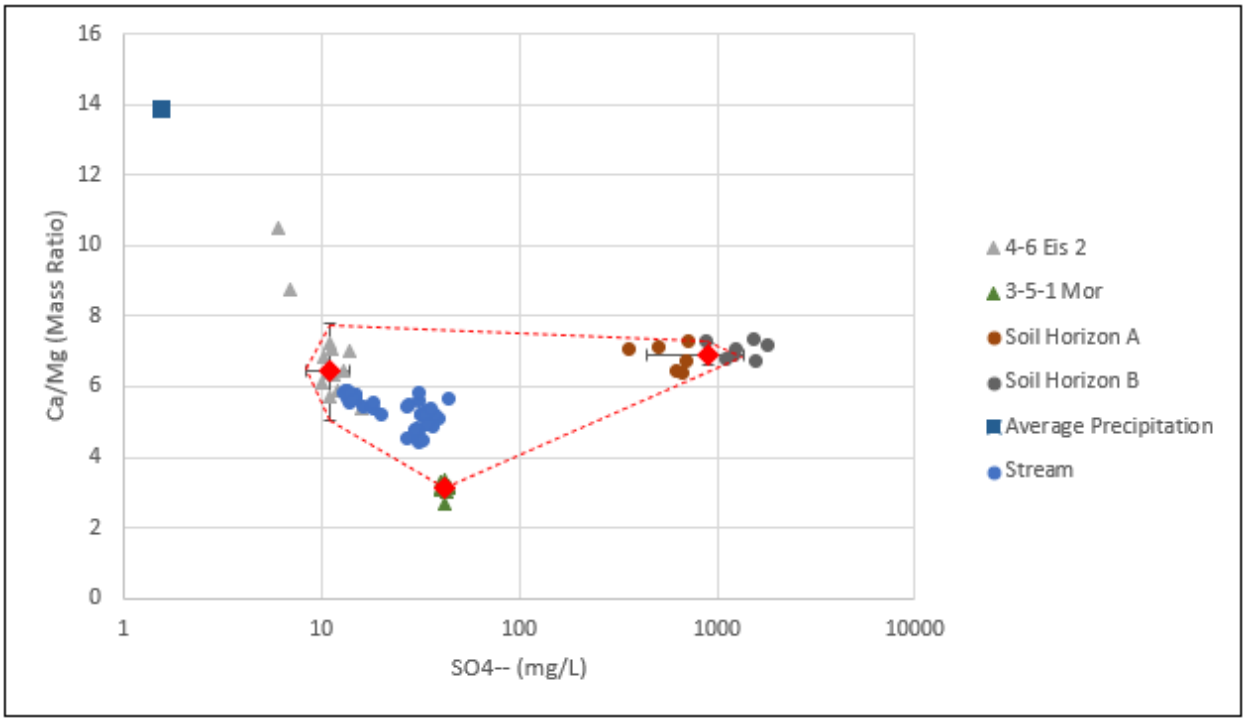

Figure 17. Bivariate plot of Ca^{2+}/Mg^{2+} vs. SO_4^{2-} for stream water samples adjusted for event water contribution and the three endmembers selected for mixing analysis. The average values of Ca^{2+}/Mg^{2+} and SO_4^{2-} that were used as the endmember compositions for each endmember are marked with red diamonds, and error bars show one standard deviation from the mean. Dashed lines denote the mixing envelope that encompasses all water samples.

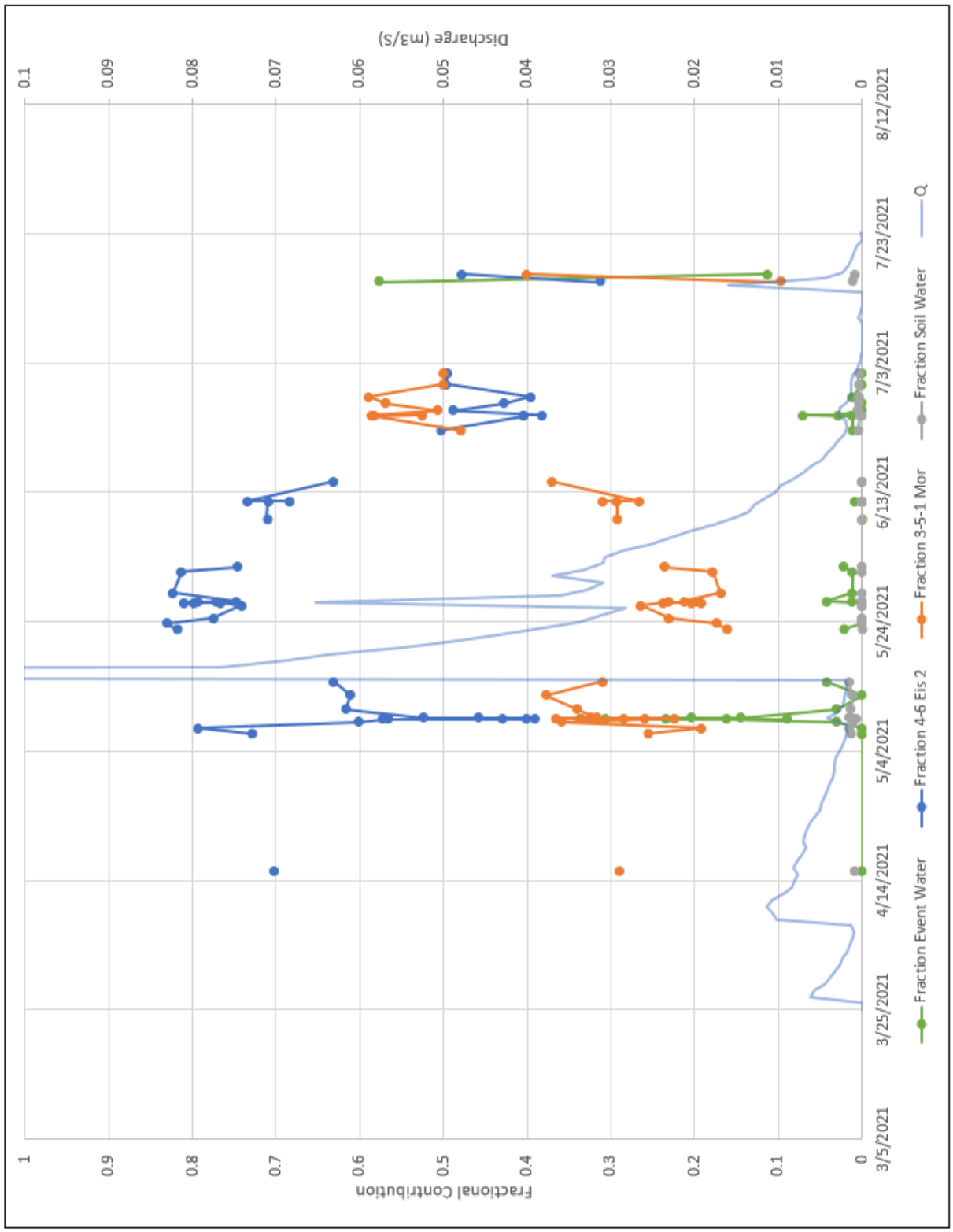

Figure 18. Fractional contributions to streamflow from event water, the two groundwater endmembers, and soil water through the sampling period. Stream discharge is marked with the light blue line for reference to flow conditions. Gaps indicate long periods of time between sampling where the dynamics were not captured.

4.6 Groundwater Elevation and Head Gradients

Figure 19 shows the water elevation in the five sampled wells from 2/23/2021 to 10/12/2021. In the deeper Morrill aquifer, the water elevation in 3-5 Mor is higher than the other two wells for the entire observed period, and the water elevation in 3-5-1 Mor is higher than 4-6 Mor for all of the observation period except for a brief window from 2/23 – 3/19. The Morrill wells all respond similarly to recharge events, except the magnitude of water level change in 4-6 Mor is higher than in the other two. During the sampling period of this study, all the Morrill wells begin with high water levels relative to their respective base levels due to spring recharge. This level gradually declines over the following weeks until the large storm on 5/16, which produces a near-instantaneous spike in water level in all three of the wells. The water level increase associated with this spike is 0.938 m in 3-5 Mor, 0.563 m in 3-5-1 Mor, and 0.339 m in 4-6 Mor. Following this spike, the water levels in all Morrill wells slowly recede over the rest of the sampling period except for small spikes associated with the storms on 5/26-5/27 and 7/15. Water levels do not reach each well's respective minimum elevation until early August.

The 4-6 Eis 1 well is representative of the low-conductivity Lower Eiss aquifer. In accordance with its low conductivity, its water levels respond very slowly to recharge events relative to the other wells. Whereas the Morrill wells had a near-instantaneous spike in water level following the 5/16 event, 4-6 Eis 1 does not achieve its maximum water level until 5/22. As further evidence of its slow response time, the well takes several days to replenish the water that we remove from it prior to sampling. This produces noticeable dips in its water elevation levels at each sampling point as shown in Figure 19.

Water levels in 4-6 Eis 2 reflect conditions in the shallowest aquifer of this study. 4-6 Eis 2 responds rapidly to recharge events relative to the other wells, with near-instantaneous spikes

in water level and quick recessions to its minimum elevation. During the sampling period, 4-6 Eis 2 begins near its minimum elevation, and the 5/16 storm caused a 1.33-meter increase in the 4-6 Eis 2 water level which then fell by 1.14 m by 5/27. Subsequent storms produced additional, smaller spikes in water level, but the well eventually returned to its minimum elevation by early June.

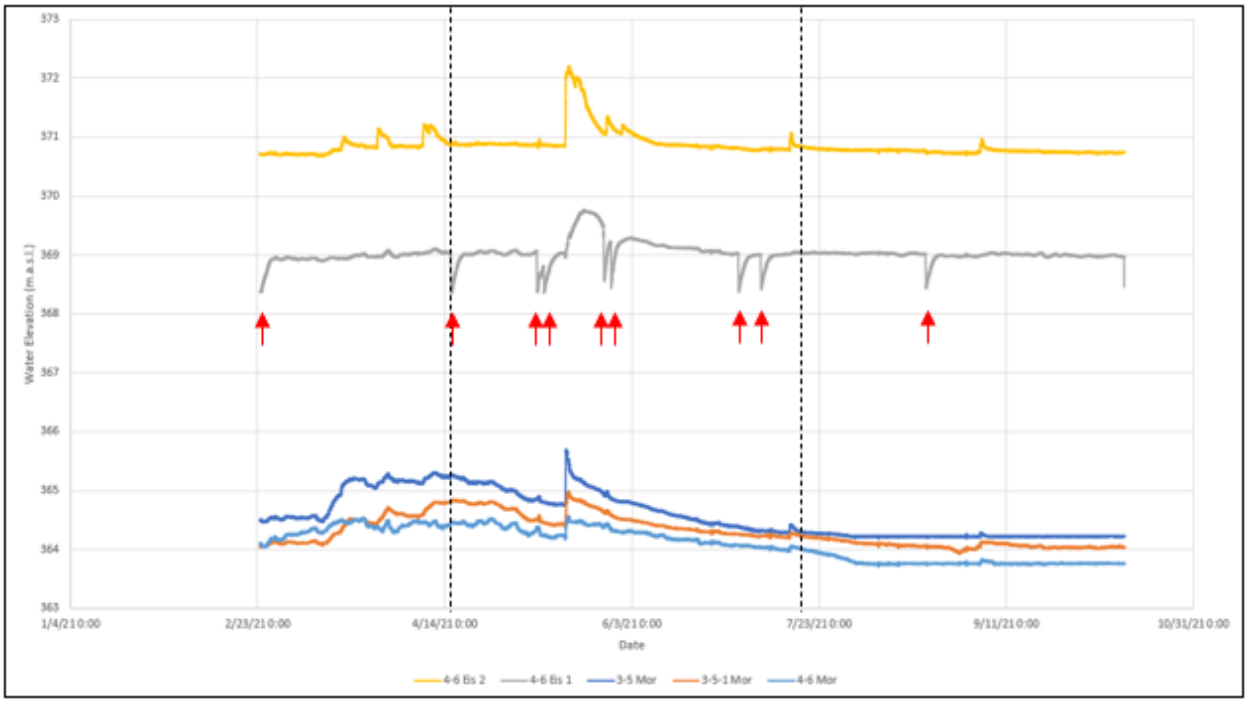

Figure 19. Water elevation within each of the sampled wells from 2/23/2021 to 10/12/2021. Black dashed lines denote the sampling period of this study. Red arrows denote when well sampling occurred, resulting in sharp declines in 4-6 Eis 1 water level which were slow to recover.

The volumetric input of water to the stream from 4-6 Eis 2 (the fractional contribution multiplied by the discharge in the stream) correlates strongly with the water elevation in the well for each stream sample ($R^2 = 0.724$, p-value from Pearson correlation < 0.001) (Figure 20). The input of water from 3-5-1 Mor shows weak to no correlation to water elevation ($R^2 = 0.320$), except when the data are separated into two time periods (Figure 21). By removing the samples from the first third of the sampling period (4/15 – 5/14, prior to the large storm on 5/16), the

correlation in the latter two thirds between input from 3-5-1 Mor and water elevation improves to $R^2 = 0.639$ (p-value from Pearson correlation < 0.001).

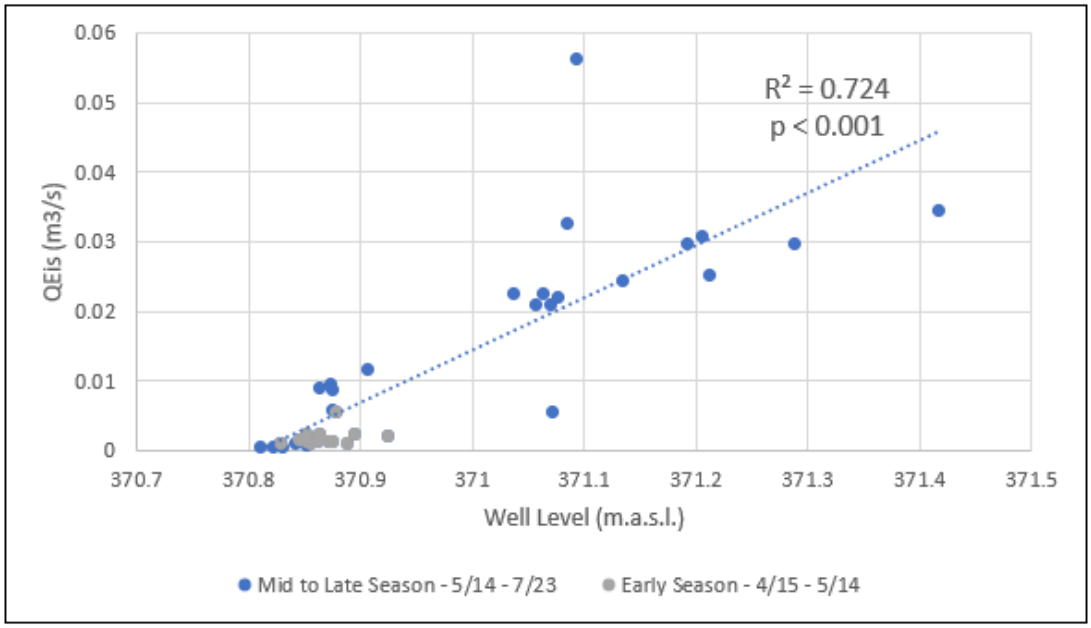

Figure 20. Relationship between volumetric input of water from the Eiss aquifer and the elevation of water in 4-6 Eis 2. Grey dots denote points from before the large storm on 5/16. Regression line is calculated for all samples, and the p-value is calculated from the Pearson correlation.

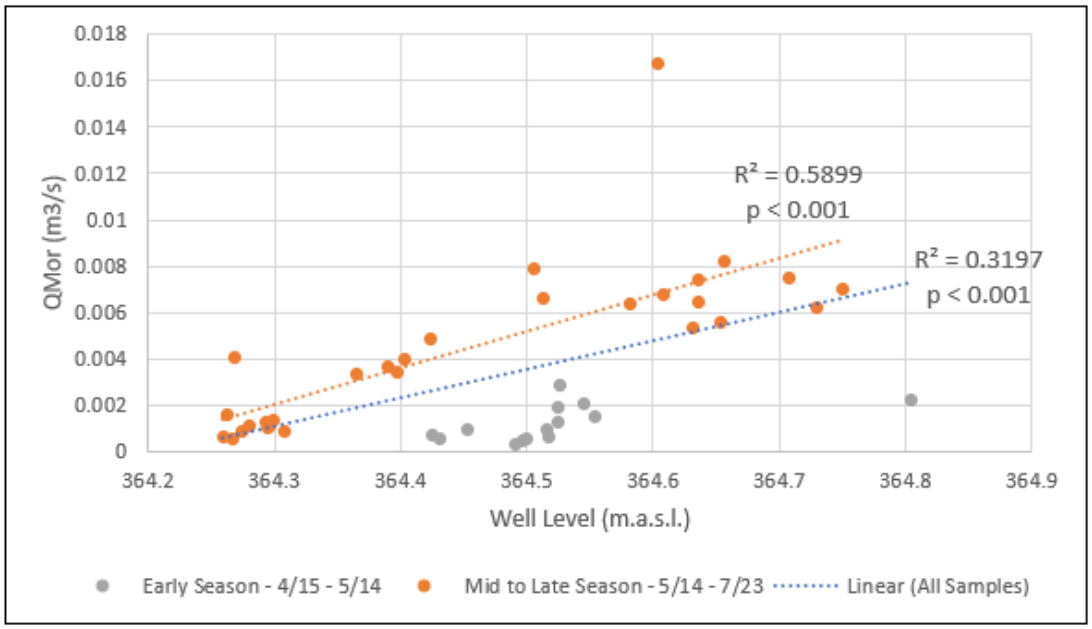

Figure 21. Relationship between volumetric input of water from the Morrill aquifer and the elevation of water in 3-5-1 Mor. The blue dotted line is the linear regression calculated from all samples, while the orange dotted line is the linear regression calculated only using the samples from after 5/14. For both regressions, the p-values are calculated from the Pearson correlation.

Figure 22 shows the magnitude and direction of the water table gradient calculated for the local area between the three Morrill wells. The data set used for these calculations was extended to include water level measurements since 2/27/2020. The magnitude and direction of the gradient correlate strongly with each other (correlation coefficient r = -0.706) in that increases in the gradient magnitude are often accompanied by shifts in the gradient direction eastward towards the stream. The year 2020 is characterized by average flow in the south-southwestern direction (bearing = 197°) at a gradient of 0.0054 m/m, while 2021 is characterized by average flow to the south-southeast (bearing = 164°) with a 57% steeper gradient of 0.0085. During a window in spring 2021 that coincides with the water elevation in 4-6 Mor exceeding that in 3-5-1 Mor (2/21 – 3/19), the gradient direction swings sharply to the west, reaching a maximum bearing of 243°. After reaching this maximum, the direction swings back towards the east to reach a bearing of 153° by the start of the sampling period on 4/15. Several sudden, sharp swings eastward appear in both 2020 and 2021 which tend to occur immediately following large precipitation events (Figure 23). Following these spikes to the east, the direction moves back towards the west at a relatively slower rate.

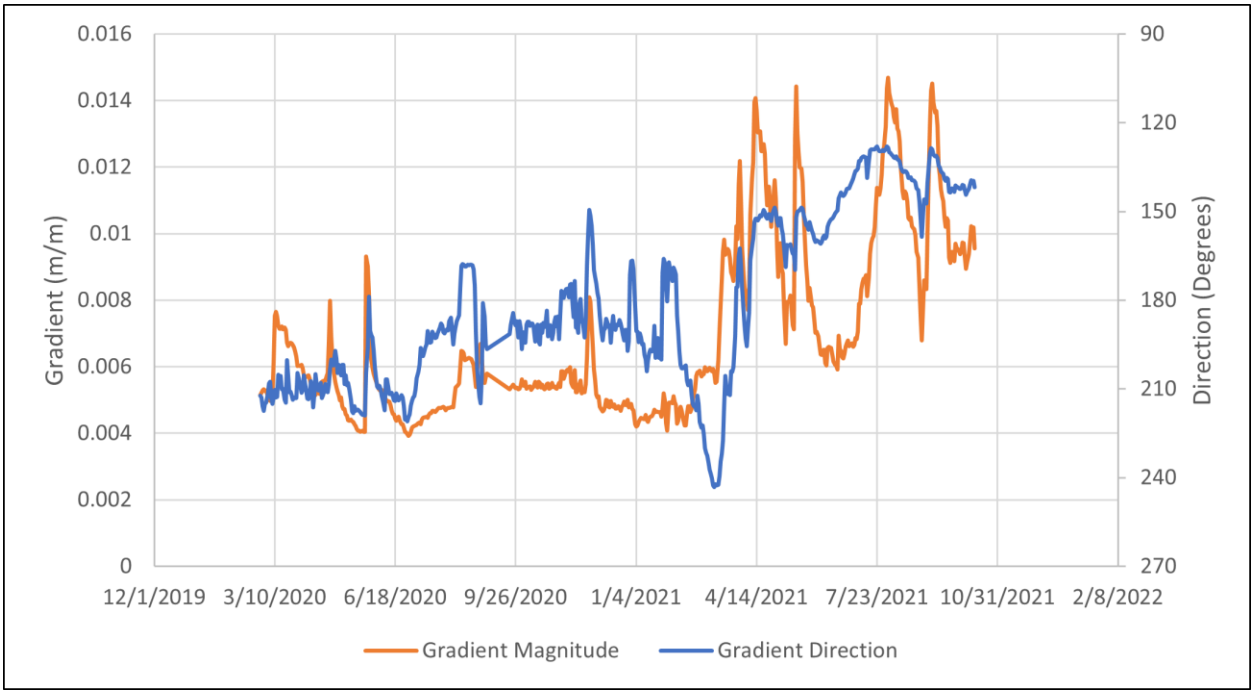

Figure 22. Magnitude and direction of the water table gradient calculated between 3-5 Mor, 3-5-1 Mor, and 4-6 Mor from 2/27/2020 to 10/12/2021. Gradient direction is plotted by bearing with due west (270°) at the bottom of the plot and due east (90°) at the top. Black dashed lines denote the sampling period of this study.

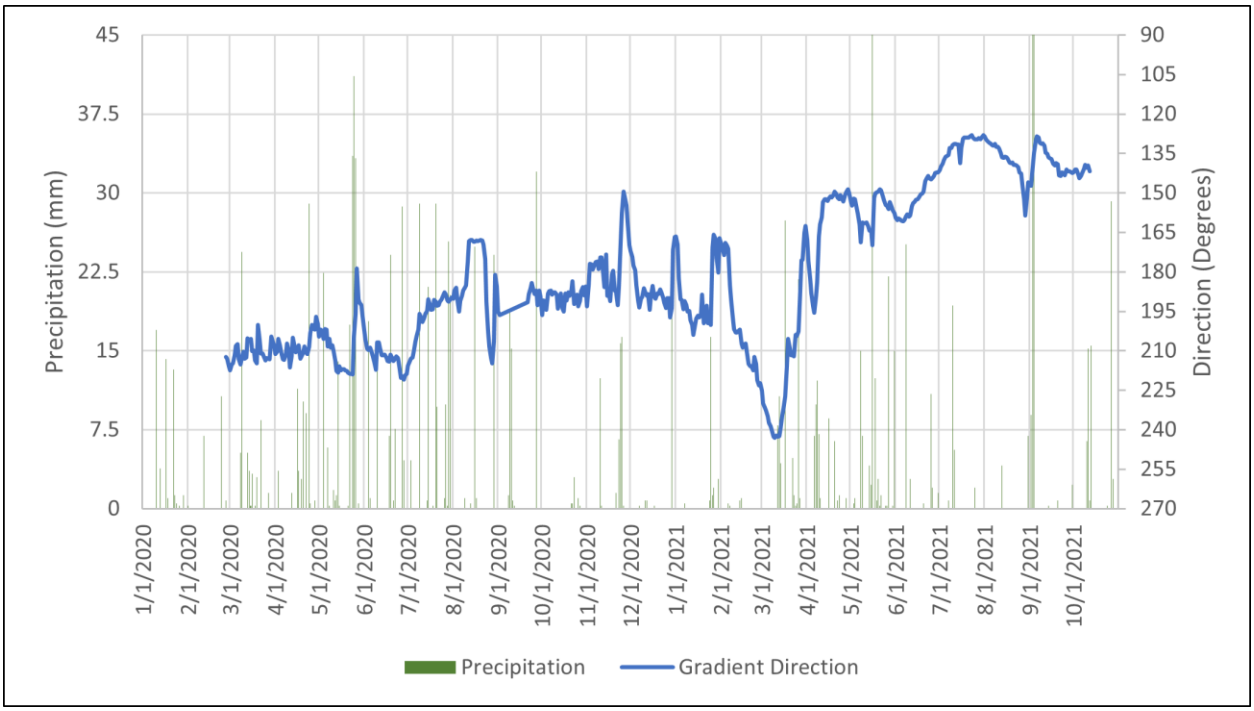

Figure 23. Direction of the water table gradient and daily precipitation amount from 2/27/2020 to 10/12/2021. Black dashed lines denote the sampling period of the study.

Chapter 4 - Discussion

The overarching goal of this study is to advance understanding of the mechanisms driving streamflow generation in the merokarst environment of N4D. To do this, we sought to quantify the relative contributions to streamflow from N4D's multiple water sources and characterize their dynamics on short time scales. Below we discuss what the results of our C-Q and mixing analyses tell us about shifting flow pathways in the catchment, and how incorporation of our groundwater elevation data might point to the influence of groundwater storage thresholds on stream intermittency.

4.1 Concentration-Discharge Behavior

Because solutes are sourced unevenly across a catchment's various environments (e.g. bedrock weathering products come mostly from deeper aquifers, nutrients and organic matter come mostly from soils, etc.), a stream's C-Q behavior can reveal much about water flow paths and streamflow generation. The results from this study (Figure 7a) show that Ca^{2+}, Mg^{2+}, and Sr^{2+} all follow chemostatic behavior. These mineral weathering products are likely sourced from large standing stocks within the groundwater, and the absence of any indication of dilution behavior implies that groundwater flow paths remain important even under high flow conditions.

Na^{+}, K^{+}, Cl^{-}, and SO_4^{2-}, on the other hand, all show varying degrees of chemodynamic behavior. Much of the variation in Na^{+}, K^{+}, and Cl^{-} is derived from the 5/8 – 5/9 storm which saw Na^{+} concentrations increase to five times its pre-storm levels, and K^{+} and Cl^{-} to over 35 times their pre-storm levels. This was the first major discharge-producing event since N4D was burned on 4/12, so the anomalously high concentrations of these solutes in the stream might be a result of the burning. Indeed, Swindle et al. (2021) showed that wildfires can increase stream cation concentrations by at least an order of magnitude by exposing topsoil and producing ash

which can later be leached into the stream. Even when excluding the samples from the 5/8 – 5/9 event, however, K^+ and Cl^- still show significant chemodynamic behavior (Figure 7b). K^+ can be generated from several different processes such as the weathering of illite or atmospheric dust, biotic cycling, and evapoconcentration of precipitation (Macpherson and Sullivan, 2019a; Sullivan et al., 2019), so the amount of K^+ that is available to be added to the stream likely varies both spatially and temporally with biotic activity and clay/dust weathering sites. Cl^- in N4D is derived exclusively from evapoconcentration of meteoric water due to the absence of halide minerals (Wood and Macpherson, 2005), so variability in the connectivity between the stream and the hillslopes can produce variability in Cl^- concentrations.

In both the full data set and the set trimmed of 5/8 – 5/9 samples, SO_4^{2-} shows strong dilution behavior. Given the very high concentrations of SO_4^{2-} in the soil water relative to the groundwater (Tsypin and Macpherson, 2012), this result suggests that shallow subsurface flow paths through the soil become less important during high flow conditions. This is in direct opposition to the shallow-and-deep hypothesis, a conceptual model commonly applied to C-Q studies which states that deep flow paths are most important during baseflow and that shallow flow paths become increasingly more important as discharge increases (Zhi et al., 2019; Stewart et al., 2022). The merokarst terrain of N4D might diverge from this typical shallow-and-deep behavior for a variety of reasons. The soil at N4D is relatively thin with an average thickness of less than 1 m (Macpherson et al., 2008), and soil is almost completely absent along many reaches of the stream, , giving way instead to exposed bedrock. Bedrock throughout the catchment is heavily fractured, and during prolonged dry periods the soil can form >3 cm macropores which accelerate deep infiltration of water (Tsypin and Macpherson, 2012). These characteristics all act to limit the potential for significant flow through the soils and prevent a

shallow-and-deep type system from emerging. The dilution behavior seen in SO_4^{2-} can instead be explained by variations in the groundwater alone – the presence of multiple perched aquifers with distinct chemical compositions means that stream chemistry might be controlled by discharge variations among the aquifers rather than flow path variations between the soil and groundwater.

A similar C-Q analysis to this one was conducted by Sullivan et al. (2019) on N4D using samples collected between May 2015 and December 2016. While their results are overall comparable to ours – chemostasis in most geogenic solutes and strong dilution behavior in SO_4^{2-} – there are a couple noticeable differences as well. First, $\frac{CV_C}{CV_Q}$ values are higher for almost all solutes in their study compared to ours. This discrepancy likely owes to the differences in sampling lengths between our two studies. By having a sampling period spanning over a year and a half, Sullivan et al. (2019) capture a much larger variety of flow conditions in the stream. Sampling across seasons and across years with different meteorological conditions would naturally create a larger variety in discharge and solute concentrations, which manifest themselves as higher $\frac{CV_C}{CV_Q}$ values. The other most significant difference between our studies is that Sullivan et al. (2019) report strong chemodynamic behavior in Mg^{2+}. Mg^{2+} is explained to have chemodynamic behavior in Sullivan et al. (2019) because it can be produced from multiple unique sources. Cation exchange sites in surface soils are thought to be the most important source of Mg^{2+} (Macpherson and Sullivan, 2019b), but illite- and chlorite-bearing mudstones as well as dolomite are also both present in N4D and have the potential to generate Mg^{2+} as a weathering product. Variations in the flow paths across these units could then result in variations in the amount of Mg^{2+} entering the stream. The fact that Mg^{2+} is chemostatic in our study suggests that the variation within these flow paths is strongly seasonal: the flow paths are stable

across our sampling period which coincides with the wet growing season, resulting in chemostatic behavior, but they become variable during the drier months of fall through early spring, resulting in the chemodynamic behavior shown in Sullivan et al. (2019).

4.2 Source Contributions to Streamflow

The primary purpose of this study was to quantify source contributions to streamflow at N4D and characterize their short-term dynamics. The results of our mixing calculations show that source contributions vary in relative strength over the growing season but are overwhelmingly dominated by groundwater sources (Figure 18). Surface runoff can comprise a significant proportion of the total stream discharge, but only during the peak of storms when the stream was dry or under low-flow conditions prior to the storm. The volumetric flow rate of surface runoff generally increases with storm intensity independent of antecedent watershed conditions, but during high flow conditions it is proportionally insignificant compared to the inputs from the groundwater sources. We hypothesize that this behavior reflects a 'fill and spill' dynamic to the hydrology of N4D: when the watershed is dry, infiltrating precipitation primarily 'fills' the subsurface storage units but does not yet discharge into the stream, causing the precipitation that does run over the surface to comprise a large proportion of streamflow. Once the watershed is sufficiently wet, however, the subsurface storage units 'spill' into the stream so that they dwarf the surface runoff in terms of fractional contribution.

The fill and spill model was initially laid out by Tromp-van Meerveld and McDonnell (2006) who showed that once a watershed achieves some threshold precipitation amount and begins to spill, total subsurface flow can increase by up to 75 times as compared to before it was filled. Sayama et al. (2011) found that fill and spill dynamics can be controlled by the surficial geology of a watershed, and Costigan et al. (2015) initially hypothesized that such a fill and spill

dynamic was operating in N4D. Costigan et al. (2015) concluded that streamflow was disconnected from precipitation inputs until the watershed attained a threshold amount of subsurface water storage, at which point streamflow and precipitation became synchronized. Our study's results on the dynamics of surface runoff seem to agree that fill and spill dynamics characterize N4D, as do our results on groundwater inputs to the stream as discussed below.

While groundwater dominates streamflow for most of the sampling period, our mixing calculations indicate that no single aquifer is responsible for the majority of streamflow across the entire sampling period. According to our results, fractional contribution of water from the Upper Eiss limestone is the highest among all sources for most of the sampling period but is overtaken by the Morrill limestone as the stream dries up. Given that the Upper Eiss is stratigraphically higher and outcrops over a larger surface area than the Morrill, it makes sense that it generally contributes more to streamflow across the sampling period. The fact that the Morrill slowly overtakes the Upper Eiss over prolonged dry periods, however, might be related to differences in the hydrologic response times of the two aquifers. Water level data (Figure 19) indicate that the Upper Eiss has a much more rapid response to precipitation than the Morrill, which we hypothesize to explain the patterns in their fractional contributions in the following manner: the Upper Eiss dominates streamflow under wet conditions by quickly routing recharge into the channel in the aftermath of precipitation, but this output rapidly dwindles in comparison to the steady trickle coming out of the Morrill which proportionally becomes more important as the Upper Eiss depletes.

Well-fitting ($R^2 > 0.7$) power law relationships between the fractional contributions of the two aquifers and discharge (F-Q relationships) support this hypothesis, albeit only for samples that were collected after the major storm on 5/16 (Figure 24). Samples prior to 5/16 show no

clear F-Q relationship, which might point to either methodological error or further evidence of fill and spill behavior at N4D. The mixing calculations that we used in this study employed the long-term, multi-year averages of tracer concentrations in each aquifer as that aquifer's endmember composition. However, actual values of SO_4^{2-} and Ca^{2+}/Mg^{2+} in the 4-6 Eis 2 well during the early part of the sampling period were over one standard deviation off from their long-term averages. This suggests that prior to the 5/16 storm, the groundwater in 4-6 Eis 2 was concentrating ions that then had to be flushed out before its composition resembled that of its endmember used in the calculations. In other words, the composition of the groundwater endmember that we used for 4-6 Eis 2 may not be applicable for samples that were collected prior to the 5/16 when the watershed was in the process of wetting up. This might ultimately have resulted in calculated fractional contributions for those early period samples being off from what is predicted by the power law F-Q relationship. Alternatively, this discrepancy can be explained by fill and spill dynamics. Assuming that the aquifers were not sufficiently filled to their 'spill point' prior to the 5/16 event, then we would expect the streamflow contributions of water from these aquifers to be disconnected from conditions within the stream. After the massive input of water into the system after 5/16, however, the subsurface units would likely become fully connected to the stream and be able to spill water into it according to the established F-Q relationship. Assuming that the effects of the shifting tracer values in the Upper Eiss endmember are minor on the calculation results, then we hypothesize that fractional contributions to streamflow from the groundwater units can be reasonably estimated from the F-Q relationship as long as the aquifers have surpassed some threshold water storage amount.

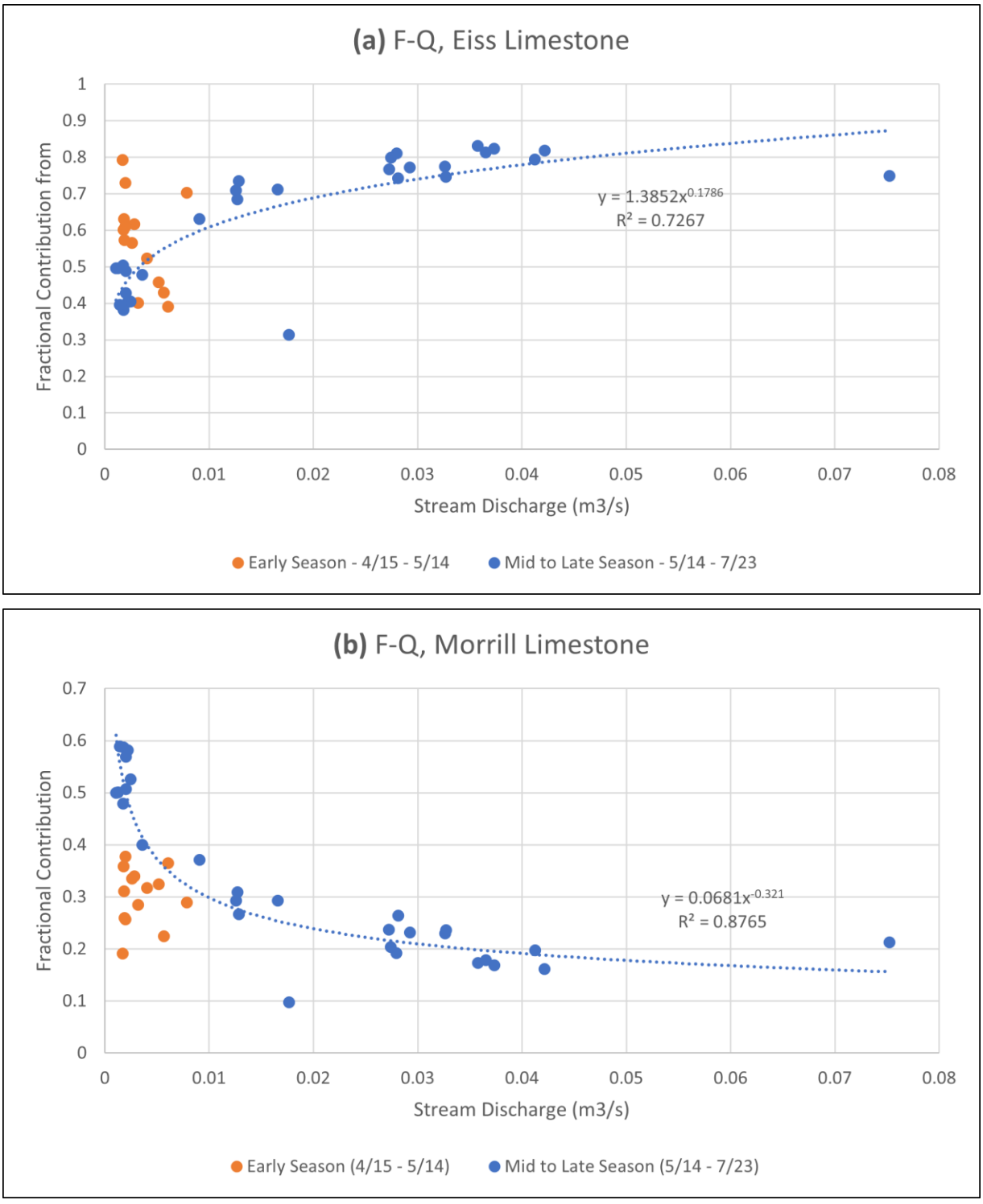

Figure 24. Relationship between fractional contribution to streamflow and stream discharge for both the Upper Eiss (a) and Morrill (b) limestones. Dotted line denotes the power law relationship fit to only the samples collected after 5/14. Orange dots denote samples which were collected prior to 5/14 and do not fit to the power law relationship.

Two other major assumptions that we made in this study are that groundwater contributions to the stream are only coming from the Upper Eiss and Morrill aquifers, and that the groundwater from the 4-6 Eis 2 and 3-5-1 Mor wells are representative of groundwater in each carbonate aquifer. The first assumption is most likely false, given that the Eiss and Morrill limestones are only the bottom two of nine total limestone units in the watershed, and previous mapping efforts have shown that there are over 50 springs throughout N4D that drain these other aquifers (Ken Ross, unpublished data, digitized by Barry (2018)). However, the fact that the Eiss and Morrill limestones are at the bottom of this stack of units means that much of the water in the higher units presumably makes its way into the Eiss and Morrill eventually, and the steeper stream channel in the upper reaches of the catchment means that these upper units have less contact area with the stream than the Eiss and Morrill do. Additionally, although there may be over 50 springs present in the catchment, they only produce water ephemerally and this water often infiltrates back into the subsurface before it reaches the stream. Furthermore, the stream samples that we collected all plot between our chosen Eiss and Morrill endmembers and variation in stream composition mostly appears to move between them (Figure 17). If other groundwater sources are contributing significant amounts of water to the stream, then they likely have chemical compositions similar to either the Eiss or Morrill endmembers and the conclusions of this study can be expanded relatively easily to include them.

The second assumption, that the groundwater we sampled is representative of the groundwater throughout each aquifer, is harder to assess due to the high degree of spatial heterogeneity seen in the merokarst carbonates of N4D (Macpherson, 1996). Our data set, which includes the samples collected in this study and the samples collected in Andrews (2021) going back to 6/25/2020, is limited to wells that consistently produced enough water for

sampling. These productive wells are not spread across a large extent of the catchment, so we are not able to ensure that solute concentrations have low spatial variability and thus that our samples are representative. Additionally, only two of the wells that are completed in the Eiss limestone are specified as being in the Upper Eiss, which is chemically and hydrogeologically distinct from the Lower Eiss (Macpherson, 1996), making it difficult to use samples from Eiss wells that are undifferentiated between the two for drawing conclusions about just the Upper unit. However, the wells that we used as our representative endmembers, 4-6 Eis 2 and 3-5-1 Mor, are the wells that displayed the lowest variations in tracer concentrations for their respective aquifer units and thus are the wells that we assume experience the least amount of mixing with other water sources. The stream samples that we collected fit well into a mixing envelope created by these selected endmembers (Figure 17), which is evidence that the stream samples are indeed some mixture of them even if the endmembers might not be perfect representations of 'pure' groundwater from their respective units.

4.3 Variations in Groundwater Head

The results of the groundwater gradient calculations shown in Figures 23 and 24 show dramatic swings in both the magnitude and direction of the groundwater gradient near the 3-5, 3-5-1, and 4-6 Mor wells. Such large changes are likely not a regional effect but a local one. Macpherson (1996) observed that a groundwater mound forms beneath the stream in the Morrill aquifer, and that this mound varies in height and position in response to the frequency and timing of recharge. Given that the mound appears to move around in the vicinity of the 3-5 Mor, 3-5-1 Mor, and 4-6 Mor wells, it is likely that large changes in the gradient are a result of shifts in the mound – east-west movement of the mound peak could explain why the gradient experiences east-west swings, and a sudden increase in gradient magnitude could be caused by moving from

the mound peak to its sloping side. The exact relationship between Morrill recharge and mound movement is yet unknown, but a rough pattern might be gleaned from the gradient calculations in this study. Large precipitation events over the last two years are generally accompanied by eastward swings and increases in gradient magnitude, so we interpret that recharge causes immediate westward movement of the mound peak relative to the 3-5, 3-5-1, and 4-6 Mor well area. Long, dry periods, on the other hand, see the gradient slowly swing back to the west, indicating a gradual return eastward of the mound peak. This pattern does not hold true in every instance, however, so further study is needed to fully understand the dynamics of the mound.

This mound, and the distortions it causes to groundwater elevations near it, is one possible explanation for the fact that samples collected prior to the 5/16 storm do not fall on the expected linear relationship between discharge from the Morrill aquifer and water elevation in the 3-5-1 Mor well (Figure 21). However, this discrepancy might also be attributed to threshold fill and spill behavior. For the pre-5/16 samples, the fact that water level is high in 3-5-1 Mor but that the Morrill is not yet discharging water into the stream at the expected rate might indicate that the stream has not yet reached full connection with this aquifer, i.e. the Morrill aquifer is still filling and not yet spilling. After the event on 5/16, however, the connection is made and then maintained even as the Morrill depletes back past the point of the initial connection. This suggests an interesting dynamic in which the threshold water storage amount only needs to be attained once and dipping back below the threshold does not completely sever the connection. Our data do not point to an exact mechanism for this, but one possibility is that water released from the aquifer when it is above the threshold is temporarily stored in shallow alluvial aquifers near the stream and is steadily released back as streamflow even after the aquifer dips back below its connection threshold. In other words, the aquifer might not actually

be spilling water into the stream when it dips back below its storage threshold, but the samples that suggest this are just comprised of 'older' water that was released when the aquifer was above its storage threshold and was delayed in reaching the sampling point. This hypothesis is consistent with a previous study by Dodds et al. (1996) who concluded that 2/3 of streamflow at N4D experiences temporary shallow subsurface storage near the stream, effectively extending the time it takes for water released by an aquifer to reach our stream sampling point.

A similar but less pronounced pattern can also be seen in the relationship between discharge from the Eiss aquifer and water elevation in the 4-6 Eis 2 well (Figure 20). Most samples collected prior to 5/16 plot well below the regression line, indicating a lower-than-expected discharge for the given well level. The fact that the pre-5/16 samples are closer to the regression line in the Eiss aquifer than in the Morrill aquifer, however, suggest that the threshold water storage needed to form a complete connection with the stream is different for each aquifer. In this case, we hypothesize that the stratigraphically higher and faster-responding Eiss aquifer has a lower threshold than the deeper, slower Morrill. This hypothesis is based on a single growing season and a limited number of wells that we sampled for this study, but future research employing data from a greater number of wells across multiple seasons could be profitable for uncovering the details and mechanisms behind the threshold behavior that we observe.

Chapter 5 - Conclusions and Implications

In this study we used mixing calculations and high-frequency sampling of stream and groundwater to quantify the contributions of different sources to streamflow at an intermittent merokarst catchment in the Konza Prairie Biological Station, USA. Our results showed that streamflow was dominated by inputs from perched limestone aquifers across most of the growing season, although surface runoff was locally important during large storms that occurred after prolonged dry periods. Well-fitting power-law relationships existed between groundwater contributions to streamflow and discharge in the stream, except for samples collected early in the sampling period. Similarly, there were well-fitting linear relationships between groundwater contributions and groundwater elevation except for those early samples. We interpreted this discrepancy between samples to be evidence of threshold-driven behavior in the catchment, where the stream channel did not become fully connected to its groundwater sources until some threshold amount of water storage in the subsurface was surpassed. Given that the merokarst landscape of the Konza Prairie is representative of the broader Flint Hills physiographic province of Kansas (Mandel, 2008), this threshold-driven behavior is likely in effect in headwater catchments throughout the region.

Because our study indicates that groundwater is the major component of streamflow and its connection to the stream is controlled by a water storage threshold, we conclude that this threshold dynamic is a major controller of stream intermittency in similar merokarst environments. Intermittent stream ecosystems are particularly vulnerable to human disturbance and global climate change (Acuña et al., 2014; Jaeger et al., 2014), but any protective management strategy is predicated on understanding the mechanisms that drive streamflow (Datry et al., 2014). Of the several possible explanations for intermittent streamflow at Konza

Prairie put forth by Costigan et al. (2015), our results point to the importance of subsurface flow paths that shift according to threshold dynamics. There is considerable room for further research in this area, however, as studies incorporating more well control and a longer sampling period could quantify this threshold for different catchments and inform management practices accordingly.

References

Acuña, V., Datry, T., Marshall, J., Barceló, D., Dahm, C.N., Ginebreda, A., McGregor, G., Sabater, S., Tockner, K., and Palmer, M.A., 2014, Why Should We Care About Temporary Waterways? Science (American Association for the Advancement of Science), v. 343, p. 1080–1081, doi:10.1126/science.1246666.

Andrews, K., 2021, Fate of CO2 in tallgrass prairie watershed underlain by merokarst bedrock, Konza Prairie, Kansas, USA:

Barry, E.R., 2018, Characterizing Groundwater Flow through Merokarst, Northeast Kansas, USA: ProQuest Dissertations Publishing.

Benda, L., Hassan, M.A., Church, M., and May, C.L., 2005, GEOMORPHOLOGY OF STEEPLAND HEADWATERS: THE TRANSITION FROM HILLSLOPES TO CHANNELS: Journal of the American Water Resources Association, v. 41, p. 835–851, doi:10.1111/j.1752-1688.2005.tb03773.x.

Blair, J., 2019, ANA01 Weekly, seasonal and annual measurement of precipitation volume and chemistry collected as part of the National Atmospheric Deposition Program at Konza Prairie:

Christophersen, N., and Hooper, R.P., 1992, Multivariate analysis of stream water chemical data: The use of principal components analysis for the end-member mixing problem: Water resources research, v. 28, p. 99–107, doi:10.1029/91WR02518.

Costigan, K.H., Daniels, M.D., and Dodds, W.K., 2015, Fundamental spatial and temporal disconnections in the hydrology of an intermittent prairie headwater network: Journal of hydrology (Amsterdam), v. 522, p. 305–316, doi:10.1016/j.jhydrol.2014.12.031.

Cowie, R.M., Knowles, J.F., Dailey, K.R., Williams, M.W., Mills, T.J., and Molotch, N.P., 2017, Sources of streamflow along a headwater catchment elevational gradient: Journal of hydrology (Amsterdam), v. 549, p. 163–178, doi:10.1016/j.jhydrol.2017.03.044.

Datry, T., Larned, S.T., and Tockner, K., 2014, Intermittent Rivers: A Challenge for Freshwater Ecology: BioScience, v. 64, p. 229–235, doi:10.1093/biosci/bit027.

Dodds, W., 2021, ASD02 Stream discharge measured at the flumes on watershed N04D at Konza Prairie:, https://portal.edirepository.org/nis/mapbrowse?packageid=knb-lter-knz.7.13.

Dodds, W.K., Blair, J.M., Henebry, G.M., Koelliker, J.K., Ramundo, R., and Tate, C.M., 1996, Nitrogen transport from tallgrass prairie watersheds: Journal of environmental quality, v. 25, p. 973–981, doi:10.2134/jeq1996.00472425002500050007x.

Dwivedi, R., Meixner, T., McIntosh, J.C., Ferré, P.A.T., Eastoe, C.J., Niu, G., Minor, R.L., Barron-Gafford, G.A., and Chorover, J., 2019, Hydrologic functioning of the deep critical

zone and contributions to streamflow in a high-elevation catchment: Testing of multiple conceptual models: Hydrological processes, v. 33, p. 476–494, doi:10.1002/hyp.13363.

Fienen, M.N., 2005, The Three-Point Problem, Vector Analysis and Extension to the N-Point Problem: Journal of geoscience education, v. 53, p. 257–262, doi:10.5408/1089-9995-53.3.257.

Ford, D.C., and Williams, P., 2007, Karst Hydrogeology and Geomorphology: Hoboken, Hoboken: Wiley.

Godsey, S.E., Kirchner, J.W., and Clow, D.W., 2009, Concentration-discharge relationships reflect chemostatic characteristics of US catchments: Hydrological processes, v. 23, p. 1844–1864, doi:10.1002/hyp.7315.

Hangen, E., Lindenlaub, M., Leibundgut, C., and von Wilpert, K., 2001, Investigating mechanisms of stormflow generation by natural tracers and hydrometric data: a small catchment study in the Black Forest, Germany: Hydrological processes, v. 15, p. 183–199, doi:10.1002/hyp.142.

Hayden, B.P., 1998, Regional climate and the distribution of tallgrass prairie: Grassland dynamics: long-term ecological research in tallgrass prairie. Oxford University Press, New York, p. 19–34.

Inamdar, S., 2011, The Use of Geochemical Mixing Models to Derive Runoff Sources and Hydrologic Flow Paths, *in* Dordrecht, Springer Netherlands, Ecological Studies, p. 163–183, doi:10.1007/978-94-007-1363-5_8.

Jaeger, K.L., Olden, J.D., and Pelland, N.A., 2014, Climate change poised to threaten hydrologic connectivity and endemic fishes in dryland streams: Proceedings of the National Academy of Sciences - PNAS, v. 111, p. 13894–13899, doi:10.1073/pnas.1320890111.

Klaus, J., and McDonnell, J.J., 2013, Hydrograph separation using stable isotopes: Review and evaluation: Journal of hydrology (Amsterdam), v. 505, p. 47–64, doi:10.1016/j.jhydrol.2013.09.006.

Leopold, L.B., 1964, Fluvial processes in geomorphology: San Francisco, W. H. Freeman, A Series of books in geology.

Liu, F., Williams, M.W., and Caine, N., 2004, Source waters and flow paths in an alpine catchment, Colorado Front Range, United States: SOURCE WATERS AND FLOW PATHS IN ALPINE CATCHMENTS: Water resources research, v. 40, doi:10.1029/2004WR003076.

Macpherson, G.L., 1996, Hydrogeology of thin limestones: the Konza Prairie Long-Term Ecological Research Site, Northeastern Kansas: Journal of hydrology (Amsterdam), v. 186, p. 191–228, doi:10.1016/S0022-1694(96)03029-6.

Macpherson, G.L., Roberts, J.A., Blair, J.M., Townsend, M.A., Fowle, D.A., and Beisner, K.R., 2008, Increasing shallow groundwater CO2 and limestone weathering, Konza Prairie, USA: Geochimica et cosmochimica acta, v. 72, p. 5581–5599, doi:10.1016/j.gca.2008.09.004.

Macpherson, G.L., and Sullivan, P.L., 2019a, Dust, impure calcite, and phytoliths: Modeled alternative sources of chemical weathering solutes in shallow groundwater: Chemical geology, v. 527, p. 118871, doi:10.1016/j.chemgeo.2018.08.007.

Macpherson, G.L., and Sullivan, P.L., 2019b, Watershed-scale chemical weathering in a merokarst terrain, northeastern Kansas, USA: Chemical geology, v. 527, p. 118988, doi:10.1016/j.chemgeo.2018.12.001.

Mandel, R.D., 2008, Buried paleoindian-age landscapes in stream valleys of the central plains, USA: The 39th Annual Binghamton Geomorphology Symposium: Fluvial Deposits and Environmental History: Geoarchaeology, Paleohydrology, and Adjustment to Environmental Change, v. 101, p. 342–361, doi:10.1016/j.geomorph.2008.05.031.

Musolff, A., Schmidt, C., Selle, B., and Fleckenstein, J.H., 2015, Catchment controls on solute export: Advances in water resources, v. 86, p. 133–146, doi:10.1016/j.advwatres.2015.09.026.

Naiman, R.J., Décamps, H. (Henri), and McClain, M.E., 2005, Riparia ecology, conservation, and management of streamside communities: Amsterdam ;, Elsevier Academic.

National Ecological Observatory Network (NEON), 2022, Stable isotopes in surface water (DP1.20206.001):, doi:10.48443/YZ7H-F560.

Nippert, J., 2021, APT01 Daily precipitation amounts measured at multiple sites across konza prairie:

Pomes, M.L., 1995, A study of the aquatic humic substances and hydrogeology in a prairie watershed: Use of humic material as a tracer of recharge through soils: ProQuest Dissertations Publishing.

Sayama, T., McDonnell, J.J., Dhakal, A., and Sullivan, K., 2011, How much water can a watershed store? Hydrological processes, v. 25, p. 3899–3908, doi:10.1002/hyp.8288.

Shook, K., and Pomeroy, J., 2012, Changes in the hydrological character of rainfall on the Canadian prairies: CHANGES IN THE HYDROLOGICAL CHARACTER OF RAINFALL ON THE PRAIRIES: Hydrological processes, v. 26, p. 1752–1766, doi:10.1002/hyp.9383.

Steward, D.R., Yang, X., Lauwo, S.Y., Staggenborg, S.A., Macpherson, G.L., and Welch, S.M., 2011, From precipitation to groundwater baseflow in a native prairie ecosystem: a regional study of the Konza LTER in the Flint Hills of Kansas, USA: Hydrology and earth system sciences, v. 15, p. 3181–3194, doi:10.5194/hess-15-3181-2011.

Stewart, B. et al., 2022, Streams as Mirrors: Reading Subsurface Water Chemistry From Stream Chemistry: Water resources research, v. 58, p. n/a, doi:10.1029/2021WR029931.

Sullivan, P.L., Stops, M.W., Macpherson, G.L., Li, L., Hirmas, D.R., and Dodds, W.K., 2019, How landscape heterogeneity governs stream water concentration-discharge behavior in carbonate terrains (Konza Prairie, USA): Chemical geology, v. 527, p. 118989, doi:10.1016/j.chemgeo.2018.12.002.

Sullivan, P.L., Zhang, C., Behm, M., Zhang, F., and Macpherson, G.L., 2020, Toward a new conceptual model for groundwater flow in merokarst systems: Insights from multiple geophysical approaches: Hydrological processes, v. 34, p. 4697–4711, doi:10.1002/hyp.13898.

Swindle, C., Shankin-Clarke, P., Meyerhof, M., Carlson, J., and Melack, J., 2021, Effects of Wildfires and Ash Leaching on Stream Chemistry in the Santa Ynez Mountains of Southern California: Water (Basel), v. 13, p. 2402, doi:10.3390/w13172402.

Thompson, S.E., Basu, N.B., Lascurain Jr, J., Aubeneau, A., and Rao, P.S.C., 2011, Relative dominance of hydrologic versus biogeochemical factors on solute export across impact gradients: Water resources research, v. 47, p. n/a, doi:10.1029/2010WR009605.

Tooth, S., 2000, Process, form and change in dryland rivers: a review of recent research: Earth-science reviews, v. 51, p. 67–107, doi:10.1016/S0012-8252(00)00014-3.

Tromp-van Meerveld, H.J., and McDonnell, J.J., 2006, Threshold relations in subsurface stormflow: 2. The fill and spill hypothesis: Water resources research, v. 42, p. W02411-n/a, doi:10.1029/2004WR003800.

Tsypin, M., and Macpherson, G.L., 2012, The effect of precipitation events on inorganic carbon in soil and shallow groundwater, Konza Prairie LTER Site, NE Kansas, USA: Applied Geochemistry, v. 27, p. 2356–2369, doi:10.1016/j.apgeochem.2012.07.008.

Veach, A.M., Dodds, W.K., and Skibbe, A., 2014, Fire and Grazing Influences on Rates of Riparian Woody Plant Expansion along Grassland Streams.:

Weary, D.J., and Doctor, D.H., 2014, Karst in the United States: A Digital Map Compilation and Database: U.S. Geological Survey Open-File Report 2014–1156.

Wood, H.K., and Macpherson, G.L., 2005, Sources of Sr and implications for weathering of limestone under tallgrass prairie, northeastern Kansas: Applied geochemistry, v. 20, p. 2325–2342, doi:10.1016/j.apgeochem.2005.08.002.

Zhi, W., Li, L., Dong, W., Brown, W., Kaye, J., Steefel, C., and Williams, K.H., 2019, Distinct Source Water Chemistry Shapes Contrasting Concentration-Discharge Patterns: Water resources research, v. 55, p. 4233–4251, doi:10.1029/2018WR024257.

Appendix A - Water Geochemistry Data

A.1 Surface Water Geochemistry

Table 3. Field measurements parameters for surface water samples collected just downstream of the discharge gauge at watershed N4D. T denotes water temperature in °C, DO denotes dissolved oxygen in mg/L, SC denotes specific conductivity in µS/cm, and Alk denotes total alkalinity in meq/L.

Date	Time	pH	T	DO	SC	Alk
4/15/2021	12:30:00 PM	6.59	13.9	9.8	481.5	5.52
5/6/2021	3:33:00 PM	6.94	19.1	8	568.5	5.7
5/7/2021	1:21:00 PM	7.04	13.7	8.1	570.9	5.25
5/8/2021	1:12:00 PM	7.38	22.8	5.4	574.6	5.72
5/8/2021	9:48:00 PM	7.02	16.9	5.9	1020	4.07
5/8/2021	10:40:00 PM	7.11	15.4	5.5	813.1	5.67
5/8/2021	11:25:00 PM	7.05	15.6	4.4	554.3	4.25
5/9/2021	12:10:00 AM	7.02	15	5.6	589.1	4.09
5/9/2021	1:20:00 AM	7.07	15.6	5.9	606.5	4.68
5/9/2021	2:41:00 AM	7.62	14.6	5.1	564.1	4.84
5/9/2021	4:42:00 AM	7.01	14	5.2	827.7	5.23
5/10/2021	10:10:00 AM	7.83	12.9	4.8	568.7	5.34
5/12/2021	4:10:00 PM	7.87	17.4	2.5	558	5.16
5/14/2021	5:38:00 PM	7.93	17.7	2	n.a.	5.49
5/22/2021	6:08:00 PM	7.97	17	1.9	524.9	5.73
5/23/2021	6:42:00 PM	7.93	16.8	8.8	564.9	5.51
5/24/2021	1:31:00 PM	8.08	17.3	8.8	500.3	5.46
5/26/2021	10:12:00 AM	8.06	16.3	8.9	505.8	5.75
5/26/2021	8:41:00 PM	7.77	15.7	8.7	508.1	5.75
5/26/2021	9:40:00 PM	7.88	15.7	9.2	506.9	5.74
5/26/2021	11:00:00 PM	7.84	15.7	8.6	493.4	5.66
5/27/2021	12:00:00 AM	7.81	15.8	8.7	505.8	5.67
5/27/2021	1:00:00 AM	7.9	15.7	8.6	489.5	5.7
5/27/2021	2:00:00 AM	7.92	15.4	8.7	475.1	5.36
5/27/2021	3:30:00 AM	7.86	15.3	8.7	491.8	5.45
5/28/2021	9:29:00 AM	7.88	13.3	9.7	496.9	5.52
5/31/2021	5:54:00 PM	7.8	14.6	9.2	502.2	5.91
6/1/2021	11:50:00 AM	7.93	14.9	9.4	508	5.64
6/8/2021	5:11:00 PM	7.84	21.5	8.8	504.6	5.61
6/11/2021	1:32:00 PM	7.61	20.6	n.a.	515	5.73
6/11/2021	2:29:00 PM	7.68	19.8	n.a.	538	5.79
6/11/2021	3:30:00 PM	7.83	20.5	n.a.	525	5.85

6/14/2021	4:19:00 PM	7.62	20.3	n.a.	535	5.85
6/22/2021	12:34:00 PM	7.46	24.2	n.a.	530	5.35
6/24/2021	7:45:00 PM	8.04	26.9	n.a.	511	5.27
6/24/2021	8:46:00 PM	8.01	26.4	n.a.	500	5.62
6/24/2021	9:40:00 PM	8.05	25.4	n.a.	515	5.62
6/25/2021	3:25:00 PM	7.87	28.1	n.a.	530	5.83
6/26/2021	7:00:00 PM	n.a.	n.a.	n.a.	n.a.	4.89
6/27/2021	4:07:00 PM	8.07	27	n.a.	510	1.44
6/29/2021	5:35:00 PM	8.15	26.4	8	526.5	4.81
7/1/2021	10:15:00 AM	8.17	21.3	8.5	540.3	5.06
7/15/2021	12:45:00 PM	8.16	21.3	7.7	441.2	4.32
7/16/2021	3:37:00 PM	8.12	24.6	8.2	558	5.74

Table 4. Anion concentrations for surface water samples. Units are in mg/L. Samples were also analyzed for Br^- and PO_4^{3-}, but concentrations of these anions were below the detection limit for every sample.

Date	Time	F-	Cl-	NO2-	NO3-	SO4--
4/15/2021	12:30:00 PM	0.4528	2.94	n.a.	0.1003	27.6685
5/6/2021	3:33:00 PM	0.4359	3.1795	n.a.	0.196	31.0243
5/7/2021	1:21:00 PM	0.4251	2.8939	n.a.	0.0125	31.2034
5/8/2021	1:12:00 PM	0.4248	3.6332	0.3509	0.1306	30.8802
5/8/2021	9:48:00 PM	0.3101	2.8743	0.0574	0.6515	23.0272
5/8/2021	10:40:00 PM	0.385	6.5425	n.a.	0.425	29.2031
5/8/2021	11:25:00 PM	0.3289	25.4861	n.a.	0.4172	24.0079
5/9/2021	12:10:00 AM	0.3217	40.0731	n.a.	0.4516	23.3113
5/9/2021	1:20:00 AM	0.3783	27.1185	n.a.	0.2937	28.6595
5/9/2021	2:41:00 AM	0.3969	11.9386	n.a.	0.1004	31.8092
5/9/2021	4:42:00 AM	0.3872	68.0165	n.a.	0.004	32.5181
5/10/2021	10:10:00 AM	0.4401	3.0114	n.a.	0.0658	33.242
5/12/2021	4:10:00 PM	0.43	2.93	n.a.	0.0139	33.2709
5/14/2021	5:38:00 PM	0.4458	3.1324	n.a.	0.0744	34.0271
5/22/2021	6:08:00 PM	0.4154	2.767	n.a.	0.1624	12.9215
5/23/2021	6:42:00 PM	0.3817	2.9121	0.065	0.0511	12.9856
5/24/2021	1:31:00 PM	0.4164	9.119	n.a.	0.595	13.511
5/26/2021	10:12:00 AM	0.3901	3.6742	0.0662	0.389	13.9454
5/26/2021	8:41:00 PM	0.4219	2.7107	0.0663	0.0037	14.7438
5/26/2021	9:40:00 PM	0.4197	2.8339	n.a.	0.0716	14.7194
5/26/2021	11:00:00 PM	0.4219	2.8541	0.0661	0.1373	14.7773
5/27/2021	12:00:00 AM	0.43	2.7332	n.a.	0.0223	15.0615
5/27/2021	1:00:00 AM	0.4229	2.9173	n.a.	0.2658	14.7418

5/27/2021	2:00:00 AM	0.3981	2.8228	0.0704	0.6842	13.9481
5/27/2021	3:30:00 AM	0.4179	2.8732	0.0696	0.344	13.9513
5/28/2021	9:29:00 AM	0.4248	9.7583	n.a.	0.5813	13.3241
5/31/2021	5:54:00 PM	0.4311	2.7493	n.a.	0.0647	13.84
6/1/2021	11:50:00 AM	0.4272	2.9016	n.a.	0.2865	13.8541
6/8/2021	5:11:00 PM	0.4205	2.7688	n.a.	n.a.	16.4767
6/11/2021	1:32:00 PM	0.4305	3.0432	n.a.	0.1433	18.1175
6/11/2021	2:29:00 PM	0.4022	2.8114	0.0754	0.098	18.1286
6/11/2021	3:30:00 PM	0.43	3.1153	0.0741	0.0875	18.4245
6/14/2021	4:19:00 PM	0.4227	3.434	0.0738	0.0978	19.9998
6/22/2021	12:34:00 PM	0.3851	2.2947	0.0264	0.4315	29.9092
6/24/2021	7:45:00 PM	0.3729	2.3073	0.0228	0.1272	31.181
6/24/2021	8:46:00 PM	0.2816	1.9434	n.a.	0.3975	25.3285
6/24/2021	9:40:00 PM	0.3656	2.3165	0.0297	0.8419	30.2259
6/25/2021	3:25:00 PM	0.3814	1.8389	0.0286	n.a.	31.5342
6/26/2021	7:00:00 PM	0.3832	2.0512	n.a.	0.0997	31.4708
6/27/2021	4:07:00 PM	0.3842	2.0113	0.027	0.0985	31.9442
6/29/2021	5:35:00 PM	0.5533	3.3165	n.a.	0.0653	29.8924
7/1/2021	10:15:00 AM	0.4679	3.4542	n.a.	0.1773	30.0957
7/15/2021	12:45:00 PM	0.3709	2.6026	0.1445	0.4494	19.3499
7/16/2021	3:37:00 PM	0.4248	2.5763	n.a.	n.a.	30.3514

Table 5. Cation concentrations for surface water samples. Units are in mg/L. Samples were also analyzed for NH_4^+, but concentrations were below the detection limit for every sample.

Date	Time	Na+	K+	Mg++	Ca++	Sr++
4/15/2021	12:30:00 PM	4.1886	0.5519	16.2037	88.7395	3.399
5/6/2021	3:33:00 PM	4.3539	1.0556	16.3607	91.4065	3.2802
5/7/2021	1:21:00 PM	4.1151	0.7972	16.2836	94.495	3.276
5/8/2021	1:12:00 PM	4.497	3.8987	16.655	86.809	3.356
5/8/2021	9:48:00 PM	3.3158	2.1698	10.8048	58.5132	2.1565
5/8/2021	10:40:00 PM	4.0586	1.6289	15.0062	78.3212	3.1166
5/8/2021	11:25:00 PM	7.5361	29.1379	12.2519	62.3528	2.4794
5/9/2021	12:10:00 AM	9.1458	42.6149	11.5151	61.3623	2.4175
5/9/2021	1:20:00 AM	8.0064	30.798	14.2858	69.5396	2.9376
5/9/2021	2:41:00 AM	5.5556	12.5757	14.934	76.1216	3.0161
5/9/2021	4:42:00 AM	14.2148	69.6525	15.7682	82.2156	3.2091
5/10/2021	10:10:00 AM	4.2533	0.9456	16.4119	86.641	3.3493
5/12/2021	4:10:00 PM	4.429	1.1788	16.5887	86.04	3.4132
5/14/2021	5:38:00 PM	5.843	1.0664	16.5476	88.7685	3.3286
5/22/2021	6:08:00 PM	3.6187	1.3827	14.8249	87.1625	3.3944
5/23/2021	6:42:00 PM	4.0141	1.5808	15.1435	88.6375	3.4914

5/24/2021	1:31:00 PM	3.5733	1.1847	15.2681	86.4965	3.2653
5/26/2021	10:12:00 AM	4.0315	0.7998	15.7978	87.7225	2.9224
5/26/2021	8:41:00 PM	3.9616	1.5168	15.5069	87.4925	3.3365
5/26/2021	9:40:00 PM	4.2945	1.791	15.3796	88.4755	3.5185
5/26/2021	11:00:00 PM	3.7417	1.2995	15.4335	89.3875	3.271
5/27/2021	12:00:00 AM	3.8076	1.3245	15.563	88.112	3.6378
5/27/2021	1:00:00 AM	3.6924	1.3195	15.0715	86.8985	3.3293
5/27/2021	2:00:00 AM	3.666	1.5223	14.5479	93.7545	3.1912
5/27/2021	3:30:00 AM	3.5894	1.4218	14.9358	85.0325	3.2148
5/28/2021	9:29:00 AM	3.6195	1.2524	14.9087	87.385	3.2475
5/31/2021	5:54:00 PM	3.6323	1.3006	15.2117	88.683	3.4095
6/1/2021	11:50:00 AM	3.3903	1.2173	15.6995	88.337	3.4574
6/8/2021	5:11:00 PM	3.5099	1.1043	16.2799	88.869	3.225
6/11/2021	1:32:00 PM	3.58	1.5661	16.4681	89.9195	3.3302
6/11/2021	2:29:00 PM	3.6677	1.4718	16.4102	88.552	3.5165
6/11/2021	3:30:00 PM	3.4867	1.2207	16.1517	89.5865	3.449
6/14/2021	4:19:00 PM	3.8713	1.3074	16.7859	87.2825	3.5532
6/22/2021	12:34:00 PM	4.138	1.2927	17.8071	85.9785	3.4084
6/24/2021	7:45:00 PM	4.0921	1.3448	17.8397	80.0005	3.4867
6/24/2021	8:46:00 PM	3.9849	1.5565	16.8495	76.8208	3.212
6/24/2021	9:40:00 PM	4.1415	1.5598	17.422	77.2205	3.4732
6/25/2021	3:25:00 PM	4.1007	1.4023	17.8359	84.852	3.4876
6/26/2021	7:00:00 PM	4.5304	1.4983	17.7914	80.9535	3.5677
6/27/2021	4:07:00 PM	4.2101	1.4883	17.9673	80.146	3.4098
6/29/2021	5:35:00 PM	4.0923	1.7394	17.408	83.1805	3.4262
7/1/2021	10:15:00 AM	2.5491	1.0787	11.3891	54.4101	2.3454
7/15/2021	12:45:00 PM	2.9826	2.336	12.4658	71.068	2.7689
7/16/2021	3:37:00 PM	4.5967	1.3495	18.1772	89.8865	3.7417

Table 6. Additional geochemical parameters for surface water samples. dD and d18O are the stable isotopes of water measured in ‰ VSMOW. NPOC is non-purgeable organic carbon in mg/L, and TN is total dissolved nitrogen in mg/L.

Date	Time	dD	d18O	NPOC	TN
4/15/2021	12:30:00 PM	n.a.	n.a.	n.a.	n.a.
5/6/2021	3:33:00 PM	-35	-5.5	n.a.	n.a.
5/7/2021	1:21:00 PM	-36	-5.6	n.a.	n.a.
5/8/2021	1:12:00 PM	-35	-5.6	n.a.	n.a.
5/8/2021	9:48:00 PM	-31	-5.1	5.814	0.5925
5/8/2021	10:40:00 PM	-33	-5.4	3.3525	0.3335
5/8/2021	11:25:00 PM	-27	-4.5	3.43	0.4753
5/9/2021	12:10:00 AM	-26	-4.4	5.445	0.659

5/9/2021	1:20:00 AM	-29	-4.8	5.124	0.4387
5/9/2021	2:41:00 AM	-30	-4.9	4.512	0.2568
5/9/2021	4:42:00 AM	-32	-5.1	3.848	0.3317
5/10/2021	10:10:00 AM	-35	-5.6	1.509	0.1493
5/12/2021	4:10:00 PM	-36	-5.7	1.698	0.1787
5/14/2021	5:38:00 PM	-35	-5.5	1.609	0.1942
5/22/2021	6:08:00 PM	-35	-5.5	1.61	0.1027
5/23/2021	6:42:00 PM	-35	-5.7	1.517	0.1738
5/24/2021	1:31:00 PM	-35	-5.7	1.867	0.3455
5/26/2021	10:12:00 AM	-35	-5.7	1.598	0.3389
5/26/2021	8:41:00 PM	-35	-5.7	2.825	0.1077
5/26/2021	9:40:00 PM	-35	-5.7	2.931	0.1096
5/26/2021	11:00:00 PM	-35	-5.7	2.596	0.1268
5/27/2021	12:00:00 AM	-35	-5.7	2.619	0.0887
5/27/2021	1:00:00 AM	-35	-5.6	2.839	0.1168
5/27/2021	2:00:00 AM	-33	-5.4	3.742	0.1246
5/27/2021	3:30:00 AM	-34	-5.5	3.238	0.1179
5/28/2021	9:29:00 AM	-35	-5.6	1.5365	0.1256
5/31/2021	5:54:00 PM	-35	-5.6	3.2855	17.32
6/1/2021	11:50:00 AM	-35	-5.5	2.857	21.7
6/8/2021	5:11:00 PM	-35	-5.6	2.387	0.0777
6/11/2021	1:32:00 PM	-35	-5.6	3.649	0.4128
6/11/2021	2:29:00 PM	-35	-5.5	2.885	0.2545
6/11/2021	3:30:00 PM	-35	-5.6	2.867	0.2327
6/14/2021	4:19:00 PM	-35	-5.6	2.842	0.55725
6/22/2021	12:34:00 PM	-35	-5.5	2.575	9.2405
6/24/2021	7:45:00 PM	-35	-5.5	2.387	0.1958
6/24/2021	8:46:00 PM	-33	-5.3	3.909	0.3654
6/24/2021	9:40:00 PM	-34	-5.5	3.634	0.3216
6/25/2021	3:25:00 PM	-35	-5.6	2.983	0.25005
6/26/2021	7:00:00 PM	-35	-5.6	2.878	0.1152
6/27/2021	4:07:00 PM	-35	-5.5	2.8	0.0896
6/29/2021	5:35:00 PM	-34	-5.4	2.6805	1.992
7/1/2021	10:15:00 AM	n.a.	n.a.	2.559	0.4679
7/15/2021	12:45:00 PM	-28	-4.9	5.616	0.50405
7/16/2021	3:37:00 PM	-34	-5.5	2.078	0.0857

Table 7. Discharge and fractional contributions from water source endmembers for each surface water sample. Discharge (Q) is measured in m^3/s.

Date	Time	Q	f Precip	f Eis	f Mor	f Soil
4/15/2021	12:30:00 PM	0.007879	0	0.702194	0.289254	0.008552
5/6/2021	3:33:00 PM	0.001961	0	0.730052	0.256527	0.013421
5/7/2021	1:21:00 PM	0.001713	0	0.792713	0.191431	0.015856
5/8/2021	1:12:00 PM	0.001782	0.02977	0.601348	0.358818	0.010065
5/8/2021	9:48:00 PM	0.001876	0.161669	0.572714	0.259501	0.006116
5/8/2021	10:40:00 PM	0.002596	0.089309	0.565664	0.335395	0.009632
5/8/2021	11:25:00 PM	0.003203	0.306389	0.401032	0.284692	0.007888
5/9/2021	12:10:00 AM	0.005646	0.336158	0.429468	0.224893	0.009481
5/9/2021	1:20:00 AM	0.006071	0.234029	0.391391	0.365031	0.009549
5/9/2021	2:41:00 AM	0.005163	0.204259	0.457392	0.3242	0.01415
5/9/2021	4:42:00 AM	0.004047	0.14472	0.523199	0.317546	0.014535
5/10/2021	10:10:00 AM	0.002843	0.02977	0.617238	0.339633	0.01336
5/12/2021	4:10:00 PM	0.001966	0	0.610703	0.377524	0.011774
5/14/2021	5:38:00 PM	0.001864	0.04259	0.631211	0.310837	0.015361
5/22/2021	6:08:00 PM	0.042168	0.022472	0.818939	0.161882	0
5/23/2021	6:42:00 PM	0.03575	0	0.830548	0.173305	0
5/24/2021	1:31:00 PM	0.032618	0	0.775173	0.230042	0
5/26/2021	10:12:00 AM	0.028131	0	0.741926	0.263969	0
5/26/2021	8:41:00 PM	0.027247	0	0.766903	0.237181	0
5/26/2021	9:40:00 PM	0.027427	0	0.799123	0.203844	0
5/26/2021	11:00:00 PM	0.027969	0	0.810398	0.192101	0
5/27/2021	12:00:00 AM	0.029254	0	0.772162	0.231368	0
5/27/2021	1:00:00 AM	0.041249	0.011236	0.793567	0.197812	0
5/27/2021	3:30:00 AM	0.07523	0.042472	0.74851	0.212693	0
5/28/2021	9:29:00 AM	0.037331	0.011236	0.822881	0.169094	0
5/31/2021	5:54:00 PM	0.036524	0.011236	0.813183	0.178541	0
6/1/2021	11:50:00 AM	0.032699	0.022472	0.745864	0.236478	0
6/8/2021	5:11:00 PM	0.016582	0	0.711338	0.292719	0
6/11/2021	1:32:00 PM	0.012581	0	0.709652	0.292569	0
6/11/2021	2:29:00 PM	0.012705	0.008929	0.684567	0.309188	0
6/11/2021	3:30:00 PM	0.012832	0	0.734386	0.266601	0
6/14/2021	4:19:00 PM	0.009065	0	0.631454	0.371372	0
6/22/2021	12:34:00 PM	0.001753	0.011628	0.504273	0.479453	0.004646
6/24/2021	7:45:00 PM	0.0022	0.011628	0.403733	0.582098	0.002541
6/24/2021	8:46:00 PM	0.002455	0.070598	0.404631	0.526214	0
6/24/2021	9:40:00 PM	0.0018	0.029485	0.382129	0.586885	0.001501
6/25/2021	3:25:00 PM	0.002027	0	0.488	0.506597	0.005404
6/26/2021	7:00:00 PM	0.002018	0	0.42778	0.569031	0.003189

6/27/2021	4:07:00 PM	0.001449	0.011628	0.395929	0.589298	0.003145
6/29/2021	5:35:00 PM	0.001079	0	0.496183	0.50002	0.003797
7/1/2021	10:15:00 AM	0.001268	0	0.495659	0.500327	0.004013
7/15/2021	12:45:00 PM	0.017658	0.577381	0.313321	0.097287	0.012011
7/16/2021	3:37:00 PM	0.003581	0.113095	0.47767	0.400296	0.008938

A.2 Groundwater Geochemistry

Data presented in this section include samples that were collected as a part of this study along with samples that were collected previously, as a part of Andrews (2021).

Table 8. Field measurements parameters for groundwater samples collected from 5 of the monitoring wells at watershed N4D. T denotes water temperature in °C, DO denotes dissolved oxygen in mg/L, SC denotes specific conductivity in µS/cm, and Alk denotes total alkalinity in meq/L.

Date	Time	pH	T	DO	SC	Alk
6/25/2020	3-5 Mor	7.04	19.4	n.a.	488.7	6.2
8/6/2020	3-5 Mor	6.65	16.7	n.a.	655.3	6.77
9/2/2020	3-5 Mor	6.89	17.7	6.7	682.8	7.08
11/2/2020	3-5 Mor	6.8	17.4	7.4	773.6	6.94
12/1/2020	3-5 Mor	6.67	13.2	7.7	761.3	6.5
02/23/2021	3-5 Mor	6.92	9.6	n.a.	689.5	6.27
04/15/2021	3-5 Mor	6.56	13.1	7.3	573.4	5.51
5/26/2021	3-5 Mor	7.35	15.8	4.8	528.2	5.74
7/7/2021	3-5 Mor	7.26	17.4	6.2	832	7.21
8/20/2021	3-5 Mor	7.05	19.1	6	634.1	6.77
8/6/2020	3-5-1 Mor	6.75	18.4	n.a.	656.4	6.34
9/21/2020	3-5-1 Mor	7.14	15.9	7.3	n.a.	6.53
10/12/2020	3-5-1 Mor	6.89	13.3	1.9	649.9	6.18
11/2/2020	3-5-1 Mor	6.94	16.2	1.7	649.4	6.27
12/1/2020	3-5-1 Mor	6.65	12.7	2.3	596.6	6.21
02/23/2021	3-5-1 Mor	6.85	13.8	n.a.	1416	6.25
04/15/2021	3-5-1 Mor	6.6	13.8	3.3	698.1	6.36
5/26/2021	3-5-1 Mor	7.3	16.8	2.1	605.7	6.31
7/7/2021	3-5-1 Mor	7.2	15.7	1.2	670	6.35
8/20/2021	3-5-1 Mor	7.18	15.3	1.7	637	6.43
8/6/2020	4-6 Eis 1	6.72	16	n.a.	581.8	5.77
9/14/2020	4-6 Eis 1	6.95	17.7	n.a.	747.5	6.72
11/2/2020	4-6 Eis 1	6.99	14.2	n.a.	736.5	5.85
12/1/2020	4-6 Eis 1	6.78	12.1	7.6	556.2	5.77

02/23/2021	4-6 Eis 1	6.8	14.6	n.a.	1216	5.95
04/15/2021	4-6 Eis 1	n.a.	n.a.	6.98	n.a.	6.17
5/8/2021	4-6 Eis 1	n.a.	n.a.	n.a.	n.a.	5.87
5/10/2021	4-6 Eis 1	7.01	13.5	5	870.5	5.77
5/26/2021	4-6 Eis 1	7.41	16.6	6.4	563.2	6.06
5/28/2021	4-6 Eis 1	7.15	12.5	5	668.5	6.04
7/1/2021	4-6 Eis 1	7.37	15.5	7.6	593.6	5.83
7/7/2021	4-6 Eis 1	7.46	15.8	6.8	607	5.85
8/20/2021	4-6 Eis 1	7.5	16.3	n.a.	544.7	6.68
8/20/2021	4-6 Eis 1	7.5	16.3	n.a.	544.7	6.68
8/6/2020	4-6 Eis 2	6.89	17.8	n.a.	566.8	7.57
9/1/2020	4-6 Eis 2	6.93	19.8	9.2	557.3	5.97
9/14/2020	4-6 Eis 2	6.81	16.5	7.1	726.3	8.31
11/2/2020	4-6 Eis 2	6.78	15.6	6.9	642.3	6.79
12/1/2020	4-6 Eis 2	6.72	13.4	5.8	671.3	6.59
02/23/2021	4-6 Eis 2	6.69	15.7	n.a.	551.2	6.28
4/15/2021	4-6 Eis 2	6.74	14.7	7.5	1855	6.06
5/8/2021	4-6 Eis 2	6.84	17.2	6.1	604.6	5.92
5/10/21	4-6 Eis 2	7.05	13.3	3.8	636.4	5.66
5/26/2021	4-6 Eis 2	7.2	16.7	5.2	506	5.6
5/28/2021	4-6 Eis 2	6.96	12.5	5.8	492.2	5.42
7/1/2021	4-6 Eis 2	7.2	15.1	6.3	561.5	3.91
7/7/2021	4-6 Eis 2	7.14	14.4	6.4	572	5.86
8/20/2021	4-6 Eis 2	7.08	17.6	6.4	532.5	5.6
6/25/2020	4-6 Mor	7.19	20.2	n.a.	459.2	6.01
8/6/2020	4-6 Mor	6.8	16.9	n.a.	625.5	6.63
9/1/2020	4-6 Mor	6.81	15.8	8.3	652.4	6.98
9/14/2020	4-6 Mor	7.03	15.4	6.5	686.2	6.91
11/2/2020	4-6 Mor	6.77	15.3	n.a.	987.9	6.99
12/1/2020	4-6 Mor	6.84	13	7.7	661.4	6.46
02/23/2021	4-6 Mor	6.98	13.6	n.a.	657.8	5.92
4/15/2021	4-6 Mor	6.42	14.2	5.3	509.5	5.63
5/8/2021	4-6 Mor	6.72	16.1	5	680.2	5.77
5/10/2021	4-6 Mor	7.13	12.9	2.5	729.3	5.86
5/26/2021	4-6 Mor	7.35	15.6	3.2	540.4	6.01
5/28/2021	4-6 Mor	7.24	13	4.4	549.6	5.85
7/1/2021	4-6 Mor	7.35	16	5.6	670.2	6.41
7/7/2021	4-6 Mor	7.2	16.2	4.7	662	7.02
8/20/2021	4-6 Mor	7.06	18.1	5.4	616.8	6.64

Table 9. Anion concentrations for groundwater samples. Units are in mg/L. Samples were also analyzed for PO_4^{3-}, but concentrations of these anions were below the detection limit for every sample.

Date	Well	F-	Cl-	NO2-	Br-	NO3-	SO4--
6/25/2020	3-5 Mor	0.4652	3.3339	0.0394	n.a.	0.2728	17.3919
8/6/2020	3-5 Mor	0.4678	3.2465	n.a.	0.0113	0.2803	23.4367
9/2/2020	3-5 Mor	0.4184	2.4502	n.a.	3.5625	0.7422	30.1834
11/2/2020	3-5 Mor	0.3831	2.8843	n.a.	n.a.	0.1388	38.2324
12/1/2020	3-5 Mor	0.4197	3.1654	n.a.	n.a.	0.1155	44.152
02/23/2021	3-5 Mor	0.7663	4.3684	n.a.	n.a.	0.203	56.7478
04/15/2021	3-5 Mor	0.492	3.2739	n.a.	n.a.	0.3354	27.3577
5/26/2021	3-5 Mor	0.5633	4.2017	n.a.	n.a.	0.1775	15.5517
7/7/2021	3-5 Mor	0.6015	3.6267	n.a.	0.0634	0.1694	22.2545
8/20/2021	3-5 Mor	0.4347	2.9533	n.a.	0.0351	0.1186	30.0569
8/6/2020	3-5-1 Mor	0.3546	4.0757	n.a.	n.a.	0.3437	42.6005
9/21/2020	3-5-1 Mor	0.4058	3.6757	n.a.	0.0092	0.4251	42.3469
10/12/2020	3-5-1 Mor	0.403	3.8832	n.a.	0.0541	0.1721	43.59
11/2/2020	3-5-1 Mor	0.3544	3.4324	n.a.	n.a.	0.1387	39.891
12/1/2020	3-5-1 Mor	0.3921	3.6999	n.a.	n.a.	0.2359	40.1122
02/23/2021	3-5-1 Mor	0.3852	4.1049	n.a.	n.a.	0.1037	43.9178
04/15/2021	3-5-1 Mor	0.3935	3.9003	n.a.	n.a.	0.1932	40.5004
5/26/2021	3-5-1 Mor	0.4609	4.8898	n.a.	0.0971	n.a.	42.8556
7/7/2021	3-5-1 Mor	0.5329	3.9464	n.a.	n.a.	0.0897	41.6845
8/20/2021	3-5-1 Mor	0.3501	3.9051	n.a.	0.029	0.0858	41.2302
8/6/2020	4-6 Eis 1	0.4228	3.2281	n.a.	n.a.	1.0684	18.8082
9/14/2020	4-6 Eis 1	0.4254	2.846	0.0998	n.a.	1.4848	21.9159
11/2/2020	4-6 Eis 1	0.4727	3.1594	n.a.	0.0067	0.9151	20.3496
12/1/2020	4-6 Eis 1	0.4698	3.058	n.a.	n.a.	1.0479	21.8192
02/23/2021	4-6 Eis 1	3.4331	11.6108	n.a.	0.0259	1.4895	19.8443
04/15/2021	4-6 Eis 1	0.7804	3.9044	n.a.	n.a.	1.6518	19.3213
5/8/2021	4-6 Eis 1	0.4315	3.3212	n.a.	n.a.	0.9521	22.8721
5/10/2021	4-6 Eis 1	0.4808	4.2053	n.a.	n.a.	1.3871	22.0815
5/26/2021	4-6 Eis 1	0.445	3.9632	n.a.	n.a.	1.6716	19.4534
5/28/2021	4-6 Eis 1	0.4777	5.7753	n.a.	n.a.	1.1661	22.2427
7/1/2021	4-6 Eis 1	0.753	4.0949	n.a.	n.a.	1.3782	19.0448
7/7/2021	4-6 Eis 1	0.6391	3.8447	0.1534	n.a.	1.7752	20.6909
8/20/2021	4-6 Eis 1	0.4315	2.7971	n.a.	n.a.	1.2998	20.0655
8/20/2021	4-6 Eis 1	0.4315	2.7971	n.a.	n.a.	1.2998	20.0655
8/6/2020	4-6 Eis 2	0.423	4.9192	n.a.	n.a.	0.677	13.9518
9/1/2020	4-6 Eis 2	0.3575	2.3909	n.a.	2.0247	0.807	12.178

9/14/2020	4-6 Eis 2	0.3847	2.3466	n.a.	0.0157	0.7295	10.9863
11/2/2020	4-6 Eis 2	0.3443	2.3525	n.a.	n.a.	0.3174	10.0979
12/1/2020	4-6 Eis 2	0.4008	2.7842	n.a.	0.0357	0.3313	11.6542
02/23/2021	4-6 Eis 2	0.4828	2.974	n.a.	n.a.	0.2935	10.8757
4/15/2021	4-6 Eis 2	0.4152	2.8165	n.a.	n.a.	0.5749	10.2046
5/8/2021	4-6 Eis 2	0.424	4.1525	n.a.	n.a.	0.6852	15.8033
5/10/21	4-6 Eis 2	0.4356	2.9976	0.0679	n.a.	0.3951	14.8372
5/26/2021	4-6 Eis 2	0.4214	3.3495	n.a.	n.a.	0.307	6.9002
5/28/2021	4-6 Eis 2	0.3718	3.0374	n.a.	n.a.	0.9283	6.099
7/1/2021	4-6 Eis 2	0.5068	3.2996	n.a.	0.0593	0.5187	12.8945
7/7/2021	4-6 Eis 2	0.5403	3.1517	n.a.	n.a.	0.4182	11.1982
8/20/2021	4-6 Eis 2	0.3622	2.9678	n.a.	n.a.	0.5861	11.0136
6/25/2020	4-6 Mor	0.426	3.7328	0.0511	n.a.	0.9795	23.1355
8/6/2020	4-6 Mor	0.4198	3.2743	n.a.	0.0076	0.4348	26.8286
9/1/2020	4-6 Mor	0.4166	2.5019	0.2111	0.0248	0.8354	28.885
9/14/2020	4-6 Mor	0.4039	2.826	n.a.	1.3203	0.4834	34.5257
11/2/2020	4-6 Mor	0.3722	60.5955	n.a.	0.0121	0.3519	38.2842
12/1/2020	4-6 Mor	0.3956	3.3288	n.a.	n.a.	0.2509	44.4666
02/23/2021	4-6 Mor	0.3631	3.0988	n.a.	n.a.	0.0719	56.9802
4/15/2021	4-6 Mor	0.468	3.2712	n.a.	n.a.	0.3106	30.8922
5/8/2021	4-6 Mor	0.4453	3.345	n.a.	n.a.	0.2882	31.3857
5/10/2021	4-6 Mor	0.4566	3.2612	n.a.	n.a.	0.0257	31.7192
5/26/2021	4-6 Mor	0.4418	3.3765	n.a.	n.a.	0.2223	24.5197
5/28/2021	4-6 Mor	0.4462	5.9026	n.a.	n.a.	0.767	21.0742
7/1/2021	4-6 Mor	0.6097	3.7597	n.a.	n.a.	0.255	24.8404
7/7/2021	4-6 Mor	0.6189	3.8542	n.a.	0.0985	0.1862	32.1025
8/20/2021	4-6 Mor	0.4125	3.3914	0.1236	0.0361	0.4916	32.019

Table 10. Cation concentrations for groundwater samples. Units are in mg/L.

Date	Well	Na+	NH4+	K+	Mg++	Ca++	Sr++
6/25/2020	3-5 Mor	4.7788	n.a.	2.3752	21.1019	98.067	4.2312
8/6/2020	3-5 Mor	5.1179	n.a.	2.0703	19.8893	99.272	4.4133
9/2/2020	3-5 Mor	4.1364	2.0797	1.043	19.3495	100.382	4.0605
11/2/2020	3-5 Mor	4.7887	n.a.	1.037	20.6244	110.646	4.7644
12/1/2020	3-5 Mor	5.3016	n.a.	1.0482	20.1045	117.324	4.8978
02/23/2021	3-5 Mor	5.5573	n.a.	1.4205	20.115	98.3645	3.8902
04/15/2021	3-5 Mor	4.8167	n.a.	1.1984	16.4244	86.036	3.5555
5/26/2021	3-5 Mor	5.0601	n.a.	0.7573	16.8156	92.1145	3.0721
7/7/2021	3-5 Mor	5.4531	n.a.	1.6041	17.4736	99.738	3.5501
8/20/2021	3-5 Mor	6.1139	0.0009	2.3601	20.0469	110.1468	3.8066
8/6/2020	3-5-1 Mor	6.8096	n.a.	1.6998	28.5385	86.7915	5.0864

9/21/2020	3-5-1 Mor	6.5058	0.25	1.9272	33.575	89.873	4.9067
10/12/2020	3-5-1 Mor	6.7182	0.9514	1.312	32.587	104.707	5.2744
11/2/2020	3-5-1 Mor	6.5183	2.2242	1.3531	27.273	84.061	4.9477
12/1/2020	3-5-1 Mor	7.1529	n.a.	1.1248	27.779	86.984	5.0359
02/23/2021	3-5-1 Mor	7.7718	n.a.	1.8523	26.7202	83.729	4.534
04/15/2021	3-5-1 Mor	7.0743	n.a.	1.5378	27.4352	90.077	4.5509
5/26/2021	3-5-1 Mor	7.7139	n.a.	1.2179	29.489	91.957	4.3044
7/7/2021	3-5-1 Mor	6.8058	n.a.	1.1724	28.4284	94.566	4.299
8/20/2021	3-5-1 Mor	6.1706	0.2915	1.5491	27.106	88.116	4.1556
8/6/2020	4-6 Eis 1	6.8698	2.2776	2.0175	24.6165	76.689	4.5019
9/14/2020	4-6 Eis 1	6.7604	1.5457	2.4027	25.509	77.2225	4.1456
11/2/2020	4-6 Eis 1	6.8711	4.7473	1.9678	24.505	75.272	4.2346
12/1/2020	4-6 Eis 1	7.2166	n.a.	1.0675	26.0305	76.0055	4.2752
02/23/2021	4-6 Eis 1	9.4802	n.a.	4.1016	22.4702	71.046	3.9162
04/15/2021	4-6 Eis 1	7.8132	n.a.	2.116	24.0702	75.4675	3.8857
5/8/2021	4-6 Eis 1	7.5541	n.a.	1.7302	25.2948	76.4772	3.904
5/10/2021	4-6 Eis 1	7.916	n.a.	2.1991	25.15	72.4008	4.0124
5/26/2021	4-6 Eis 1	8.0914	n.a.	1.3694	26.109	78.0745	3.7041
5/28/2021	4-6 Eis 1	8.3464	n.a.	2.4002	27.8204	77.3748	4.4829
7/1/2021	4-6 Eis 1	6.6929	n.a.	1.8536	25.3364	77.9456	4.353
7/7/2021	4-6 Eis 1	7.8281	n.a.	1.6041	25.2282	88.743	3.9341
8/20/2021	4-6 Eis 1	6.6607	0.2778	1.7351	25.0828	78.332	3.5365
8/20/2021	4-6 Eis 1	6.6607	0.2778	1.7351	25.0828	78.332	3.5365
8/6/2020	4-6 Eis 2	4.6865	n.a.	3.4379	15.1032	105.65	3.9155
9/1/2020	4-6 Eis 2	2.9027	0.2948	0.6223	14.9176	87.796	3.3344
9/14/2020	4-6 Eis 2	3.4552	1.6842	1.2337	15.814	90.022	3.6374
11/2/2020	4-6 Eis 2	3.8044	0.5353	0.7195	16.2258	99.072	3.7485
12/1/2020	4-6 Eis 2	6.7038	n.a.	0.472	15.3123	97.078	3.7223
02/23/2021	4-6 Eis 2	7.0853	n.a.	1.0961	14.6163	93.7445	3.1475
4/15/2021	4-6 Eis 2	4.0086	n.a.	1.0556	13.6999	93.751	3.1436
5/8/2021	4-6 Eis 2	6.1203	n.a.	4.6929	16.0875	86.9505	3.1732
5/10/21	4-6 Eis 2	4.0845	n.a.	1.0426	15.4229	87.5485	3.2453
5/26/2021	4-6 Eis 2	3.9703	n.a.	0.5124	10.5305	92.178	2.5306
5/28/2021	4-6 Eis 2	3.0333	n.a.	0.9619	9.132	95.969	2.821
7/1/2021	4-6 Eis 2	4.8212	n.a.	1.4291	14.1053	90.8495	2.8974
7/7/2021	4-6 Eis 2	4.0268	n.a.	0.7356	13.7068	96.987	3.0484
8/20/2021	4-6 Eis 2	3.8364	1.3082	1.8384	12.5204	90.3804	2.4031
6/25/2020	4-6 Mor	4.3869	2.6011	2.5066	19.1984	109.743	4.0013
8/6/2020	4-6 Mor	5.0142	n.a.	1.812	22.275	99.581	4.4501
9/1/2020	4-6 Mor	4.4166	1.6826	1.1061	20.3561	95.245	4.5129
9/14/2020	4-6 Mor	4.9162	1.4392	1.1572	26.872	125.496	4.6534

11/2/2020	4-6 Mor	12.7158	3.8594	58.633	21.672	100.503	4.8403
12/1/2020	4-6 Mor	5.4193	n.a.	0.7632	17.754	80.946	4.7159
02/23/2021	4-6 Mor	4.9445	n.a.	0.7046	19.9974	98.597	3.8236
4/15/2021	4-6 Mor	4.918	n.a.	0.7625	17.915	86.6195	3.6369
5/8/2021	4-6 Mor	5.0949	n.a.	1.2217	18.163	88.2735	3.3057
5/10/2021	4-6 Mor	4.9522	n.a.	1.0942	18.1395	89.223	3.7862
5/26/2021	4-6 Mor	5.7548	n.a.	0.7011	20.0678	86.299	3.4534
5/28/2021	4-6 Mor	5.2847	n.a.	1.6162	18.3447	86.907	3.8167
7/1/2021	4-6 Mor	4.9379	n.a.	1.4977	19.2087	97.075	3.9855
7/7/2021	4-6 Mor	5.9099	n.a.	1.0948	20.7126	95.8415	4.0013
8/20/2021	4-6 Mor	5.1534	0.1466	1.474	20.9668	102.8375	3.8864

Table 11. Additional geochemical parameters for groundwater samples. dD and d18O are the stable isotopes of water measured in ‰ VSMOW. NPOC is non-purgeable organic carbon in mg/L, and TN is total dissolved nitrogen in mg/L.

Date	Well	dD	d18O	NPOC	TN
5/8/2021	4-6 Eis 1	-37	-5.8	n.a.	n.a.
5/10/2021	4-6 Eis 1	-38	-6	n.a.	n.a.
5/26/2021	4-6 Eis 1	-38	-6.2	2.727	0.5166
5/28/2021	4-6 Eis 1	-37	-5.8	1.794	0.4908
7/1/2021	4-6 Eis 1	n.a.	n.a.	3.423	0.74065
5/8/2021	4-6 Eis 2	-36	-5.7	n.a.	n.a.
5/10/21	4-6 Eis 2	-36	-5.7	6.207	0.3419
5/26/2021	4-6 Eis 2	-34	-5.5	20.27	0.6756
5/28/2021	4-6 Eis 2	-34	-5.3	2.497	0.36715
7/1/2021	4-6 Eis 2	-35	-5.6	11.11	0.59385
5/8/2021	4-6 Mor	-36	-5.7	n.a.	n.a.
5/10/2021	4-6 Mor	-36	-5.7	2.678	0.1932
5/26/2021	4-6 Mor	-35	-5.7	9.954	0.3345
5/28/2021	4-6 Mor	-34	-5.3	2.529667	0.2874
7/1/2021	4-6 Mor	-36	-5.6	2.995	0.37535

Appendix B - Concentration-Discharge Results

Table 12. Values of CV_c/CV_q and the *b* parameter from $C = aQ^b$ for each solute in the surface water samples.

Solute	CVc/CVq	b
F-	0.09988	0.002544
Cl-	0.520813	0.088625
SO4--	0.368112	-0.25981
Na+	0.138424	-0.03777
K+	0.234787	0.018954
Mg++	0.092107	-0.03125
Ca++	0.085349	0.025685
Sr++	0.076058	0.000797